Molecular Therapy
Original Article

Neat1 promotes acute kidney injury to chronic kidney disease by facilitating tubular epithelial cells apoptosis via sequestering *miR-129-5p*

Tongtong Ma,[1] Hongwei Li,[2] Hui Liu,[3] Yili Peng,[2] Tong Lin,[2] Zhiya Deng,[1] Nan Jia,[2] Zhongqing Chen,[1] and Peng Wang[2]

[1]Department of Critical Care Medicine, Nanfang Hospital, Southern Medical University, Guangzhou 510515, China; [2]Division of Nephrology, Nanfang Hospital, Southern Medical University, National Clinical Research Center for Kidney Disease, State Key Laboratory of Organ Failure Research, Guangdong Provincial Institute of Nephrology, Guangdong Provincial Key Laboratory of Renal Failure Research, Guangzhou 510515, China; [3]Department of Anesthesiology, The First Affiliated Hospital of Guangzhou Medical University, Guangzhou 510120, China

Acute kidney injury (AKI) is increasingly identified as a crucial risk factor for progression to CKD. However, the factors governing AKI to CKD progression remain largely unknown. By high-throughput RNA sequencing, we found that *Neat1_2*, a transcript variant of *Neat1*, was upregulated in 40-min ischemia/reperfusion injury (IRI), which resulted in the development of renal fibrotic lesions. The upregulation of *Neat1_2* in hypoxia-treated TECs was attributed to p53 transcriptional regulation. Gain- and loss-of-function studies, both *in vitro* and *in vivo*, demonstrated that *Neat1_2* promoted apoptosis of injured TECs induced by IRI and caused tubulointerstitial inflammation and fibrosis. Mechanistically, *Neat1_2* shares miRNA response elements with *FADD*, *CASP-8*, and *CASP-3*. *Neat1_2* competitively binds to *miR-129-5p* and prevents *miR-129-5p* from decreasing the levels of *FADD*, *CASP-8*, and *CASP-3*, and ultimately facilitates TEC apoptosis. Increased expression of *Neat1_2* associated with kidney injury and TEC apoptosis was recapitulated in human AKI, highlighting its clinical relevance. These findings suggest that preventing TEC apoptosis by hindering *Neat1_2* expression may be a potential therapeutic strategy for AKI to CKD progression.

INTRODUCTION

Chronic kidney disease (CKD) is progressive and irreversible after renal function drops below a certain threshold, and there is currently no decisive therapy.[1] Progressive tubulointerstitial fibrosis is a common characteristic of CKD leading to end-stage renal disease (ESRD).[2] Acute kidney injury (AKI) is a clinical condition characterized by a rapid decline in renal function and has long been regarded as a completely reversible condition. However, recent studies have shown that patients who survive an episode of AKI may suffer from persistent subclinical kidney injury, placing them at higher risk for progression to CKD, ESRD, and death.[3–5]

The severity and frequency of AKI determine whether the injury leads to CKD.[6] Tubular epithelial cells (TECs), which make up the bulk of the renal parenchyma, are the initial targets for ischemia/reperfusion (I/R)-induced renal injury and are vulnerable to varieties of injuries, including hypoxia, senescence, proteinuria, toxins, and metabolic disorders.[7] Accumulating evidence shows that injured TECs, which can result in apoptosis, are considered a critical element that initiates progressive fibrosis.[8,9] Activation of the FasL/Fas-related pathway is critical for I/R-induced cell apoptosis and organ damage.[10,11] Activated Fas receptor recruits and activates caspase-8 by binding to FADD (Fas-associated protein with death domain), leading to the cleavage of caspase-3/-7, which initiates the morphological changes of apoptosis.[12] It has been widely recognized that the activation of the Fas receptor contributes to TEC apoptosis and that knockout of the Fas receptor protects the kidney against I/R-induced injury.[13,14] Therefore, research on TEC apoptosis may provide a promising therapeutic target for preventing AKI to CKD progression.

Long non-coding RNAs (lncRNAs) are a cluster of RNA molecules (longer than 200 nt) that may regulate gene expression through diverse functional mechanisms. They can interact with protein targets [15–17] or sequester miRNA activity as competing endogenous RNAs.[18] Emerging evidence has shown that lncRNAs play a critical role in the pathogenesis of AKI.[19,20] However, there is limited knowledge about the role of lncRNAs in the progression of AKI to CKD.

In this study, we investigated the potential role of lncRNAs involved in the progression of AKI to CKD and their underlying mechanisms. We found that lncRNA *Neat1_2* contributed to the progression of AKI to CKD by promoting TEC apoptosis. This discovery expands on our understanding of the regulation of TEC apoptosis and AKI

Received 6 November 2021; accepted 21 May 2022;
https://doi.org/10.1016/j.ymthe.2022.05.019.

Correspondence: Peng Wang, Division of Nephrology, Nanfang Hospital, Southern Medical University, National Clinical Research Center for Kidney Disease, State Key Laboratory of Organ Failure Research, Guangdong Provincial Institute of Nephrology, Guangdong Provincial Key Laboratory of Renal Failure Research, Guangzhou 510515, China.
E-mail: wangpeng7730230@smu.edu.cn

Please cite this article in press as: Ma et al., *Neat1* promotes acute kidney injury to chronic kidney disease by facilitating tubular epithelial cells apoptosis via sequestering *miR-129-5p*, Molecular Therapy (2022), https://doi.org/10.1016/j.ymthe.2022.05.019

progression, providing a potential new therapeutic target for renal fibrosis.

RESULTS

lncRNA *Neat1_2* is upregulated in TECs from mice exposed to severe ischemic reperfusion injury (IRI)

The kidney has an inherent ability to recover from acute injury; however, severe injury can result in CKD and fibrosis.[21,22] To study the role of lncRNAs in renal TECs after severe injury, severe or mild ischemic reperfusion injury (IRI) was established in mice by 40 or 20 min, respectively, of bilateral renal IRI. As previously described,[6,22] severe IRI caused severe acute tubular injury, whereas mild IRI induced mild acute tubular injury, from which subjects recovered 7 days post-injury (Figures S1A and S1B). Moreover, severe IRI caused the development of CKD, as shown by progressive tubulointerstitial fibrosis since day 7 post-injury (Figures S1C and S2D), deposition of extracellular matrix synthesis (Figures S1E and S1F), and the serum creatinine remained above normal level for at least 42 days post-injury (Figure S1G).

Screening of the differentially expressed lncRNAs between IRI and the sham group was performed by high-throughput sequencing with the isolated tubules from mice. The lncRNA clustering showed that 8 lncRNAs were upregulated and 46 were downregulated by >2-fold between severe and mild IRI (Figure 1A; Tables S1 and S2). We selected the candidate lncRNA *Neat1* for the following reasons: (1) *Neat1* is highly conservative between mice and humans, (2) *Neat1* has the highest constitutional expression level (fragments per kilobase of transcript per million mapped reads [FPKM] 70.02 ± 30.90) in mouse renal tubules, and (3) *Neat1* is an intergenic lncRNA that does not overlap with protein-coding genes, avoiding off-target effects through the manipulation of *Neat1*. Bioinformatics analysis reveals that *Neat1* (NCBI Gene ID: 66961) is transcribed into 2 isoforms, 3.2k-nt *Neat1_1* (NR_003513) and 20k-nt *Neat1_2* (NR_131212) (Figure S1H). To determine the dominating transcript in IRI-injured kidney, northern blot was performed in mouse injured renal tissues. The results showed that the expression level of *Neat1_2* transcript was more abundant than that of the *Neat1_1* transcript in IRI mouse kidneys (Figure 1B). To further validate the upregulation of *Neat1_2*, quantitative real-time polymerase chain reaction (qPCR) showed that *Neat1_2* was upregulated in isolated tubules from severe IRI mice (Figure 1C) and hypoxia-treated human and mouse TECs, which is a model to mimic IRI in TECs *in vitro* (Figures 1D and 1E). To characterize the localization of *Neat1_2*, fluorescence *in situ* hybridization (FISH) was performed in TECs treated under different conditions. Compared with normal TECs, hypoxia-treated cells contained more *Neat1_2* in the cytoplasm (Figure 1F), which were verified by qPCR of the cytoplasmic and nuclear fractions (Figure 1G). Similarly, FISH in kidney sections from IRI mice demonstrated that *Neat1_2* was predominantly upregulated in proximal tubules of severe IRI mice, as revealed by the colocalization of *Neat1_2* and the marker of proximal tubules (*Lotus tetragonolobus*) (Figure S1I). *Neat1_2* was expressed in both the cytoplasm and the nucleus of TECs from 1 to 42 days post-IRI (Figures S1J and S1K). While in sham and mild IRI mice, *Neat1_2* was dominantly expressed in the nucleus (Figures 1H and 1I). These observations suggest that *Neat1_2* is released from the nucleus to the cytoplasm during severe TEC injury.

Neat1_2 is a transcription target of p53 in TECs from mice exposed to severe IRI

Burgeoning evidence shows that transcription factors (TFs) can play indispensable roles in the upregulation of lncRNAs.[16,23,24] We therefore conducted bioinformatics analysis by using the ChIPBase database[25] to screen for TFs responsible for *Neat1_2* upregulation (Data S1). To narrow down the candidate TFs, DNA pull-down followed by mass spectrometry was performed (Figure S1L). We took the intersetion of the predicted TFs and the TFs identified by mass spectrometry (Figure 1J; Data S2). The results demonstrated that p53 and RelA bound to the promoter sequence of Neat1_2. To further confirm the role of p53 and RelA in dominating the upregulation of *Neat1_2* in TECs treated with hypoxia, *p53* and *RelA* were knocked down separately (Figures S1M–S1P). The results showed that knockdown of *p53*, but not *RelA*, decreased *Neat1_2* expression in TECs, in the presence or absence of hypoxia treatment (Figures S1Q and S1R).

To validate the findings, we cloned the promoter region of *Neat1_2* between −1 and −2,000 bp into a pGL3 vector. Luciferase reporter assays demonstrated that knocking down *p53* inhibited *Neat1_2* promoter activity (Figure 1K), and these results suggested that the transcription of *Neat1_2* was p53 dependent. According to the JASPAR CORE 2020 database,[26] there is one predicted potential p53 binding site in the promoter region of *Neat1_2* (−1,459 to −1,475 bp upstream in human genome build hg38). We further performed chromatin immunoprecipitation (ChIP) analysis with an anti-p53 antibody to demonstrate whether p53 could occupy the *Neat1_2* promoter in TECs. The ChIP assay demonstrated the interaction between p53 and the promoter region of *Neat1_2*, indicating that *Neat1_2* is a direct target of p53 (Figure 1L). A series of pGL3 reporter plasmids containing truncated mutations between −2,000 and −1 bp of the *Neat1_2* promoter were constructed (Figure 1M). Luciferase reporter assays showed that the mutants without the predicted p53 binding site (−1,459 to −1,475 bp) lost transcriptional activity when cells were treated with hypoxia. Further validation of the binding site is indispensable for *Neat1_2* transcription upon hypoxia treatment. Point mutations of the p53 binding site were established, and the results showed that mutations of this binding site (−1,459 to −1,475 bp) reduced luciferase activity (Figure 1N). These data suggest that p53 upregulates the expression of *Neat1_2* by directly binding to the promoter of *Neat1_2*.

To explore whether p53 contributes to the upregulation of *Neat1_2* *in vivo*, we first verified that p53 was activated in injured TECs *in vitro* (Figures S1M and S1N) and in isolated tubules from severe IRI mice (Figures S1S and S1T). Then, one group of IRI mice was given intraperitoneally (i.p.) with pifithrin-α (PIF-α), a p53 inhibitor,[27] 12 h before IRI induction. PIF-α treatment decreased the expression of *Neat1_2* at days 1, 3, and 7 post-IRI (Figure S1U).

Please cite this article in press as: Ma et al., *Neat1* promotes acute kidney injury to chronic kidney disease by facilitating tubular epithelial cells apoptosis via sequestering *miR-129-5p*, Molecular Therapy (2022), https://doi.org/10.1016/j.ymthe.2022.05.019

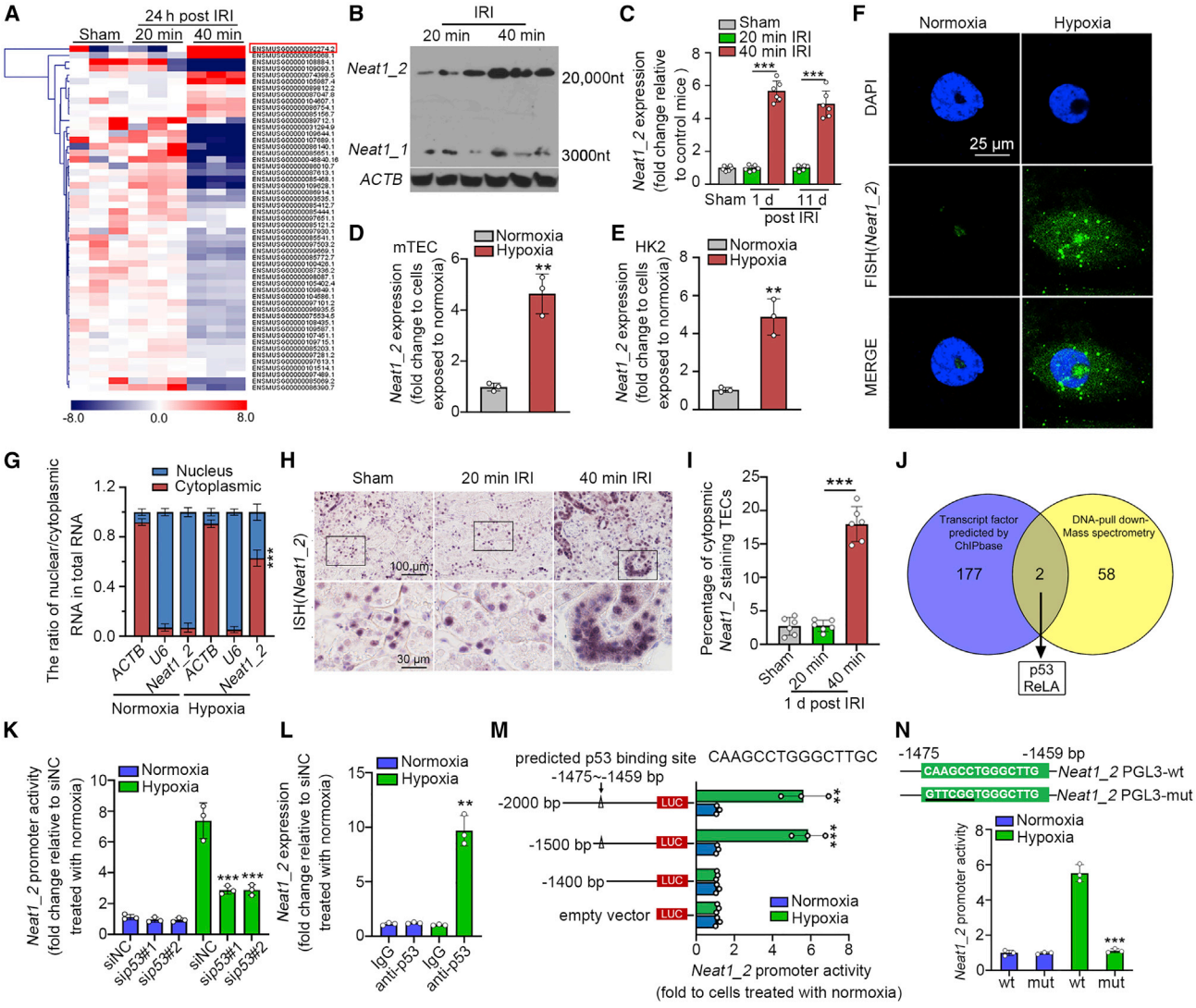

Figure 1. LncRNA *Neat1_2* is upregulated by p53 transcription in TECs from mice exposed to severe IRI

(A) Clustered heatmap of the differentially expressed lncRNAs in isolated tubules from sham and IRI mice (n = 3). (B) Northern blots for the 2 transcript variants of *Neat1* in isolated tubules from 20- or 40-min IRI mice (n = 3). (C) Expression of *Neat1_2* in isolated tubules from sham and IRI mice, assayed by qPCR. (D and E) Expression of *Neat1_2* in mouse tubular epithelial cells (mTECs) (D) and HK2 cells (E) treated with hypoxia (1% oxygen) for 24 h. (F) The subcellular location of *Neat1_2* in normoxia or hypoxia-treated HK2 cells was analyzed by RNA-FISH. Scale bar, 25 μm. (G) Normoxia- or hypoxia-treated HK2 cells were analyzed for cytoplasmic and nuclear percentage of *Neat1_2*. (H and I) Representative images of *in situ* hybridization of *Neat1_2* expression in kidneys from sham or IRI mice (H) and the percentage of cytoplasmic *Neat1_2* staining TECs (I), Scale bars, 100 μm in the upper images and 30 μm in the lower images. (J) A Venn diagram showing potential transcription factors associated with *Neat1_2*. Transcription factors (p53 and Rela) were selected by using DNA pull down followed by liquid chromatography-tandem mass spectrometry as well as ChIPBase. (K) Knockdown of *p53* decreased the *Neat1_2* transcription activity in luciferase reporter assays. (L) ChIP assays showing p53 occupied at the *Neat1_2* promoter in HK2 cells. (M) Luciferase reporter assays for HK2 cells that were transfected with reporter plasmids containing truncated *Neat1_2* promoters and then treated with hypoxia for 24 h. (N) Mutation of p53 binding site rescued *Neat1_2* transcription in *luciferase* reporter assays. The data are presented as means ± SDs. A Student's t test was used for the comparison of 2 groups. ANOVA was used for comparison among multiple groups. **p < 0.01, ***p < 0.001.

Upregulation of *Neat1_2* activates TEC apoptosis

The common pathological characteristics of AKI are apoptosis of resident renal cells and excessive inflammation, which will lead to progressive fibrosis.[8] By conducting mRNA sequencing (mRNA-seq) and Gene Ontology (GO) analysis in tubules isolated from mild or severe IRI, a series of apoptosis-associated genes were found to be markedly upregulated in TECs from severe IRI mice (Figures S2A and S2B). Indeed, apoptotic TECs were dramatically increased in severe IRI mice, as assayed by TUNEL staining (Figures S2C and S2D).

Please cite this article in press as: Ma et al., *Neat1* promotes acute kidney injury to chronic kidney disease by facilitating tubular epithelial cells apoptosis via sequestering *miR-129-5p*, Molecular Therapy (2022), https://doi.org/10.1016/j.ymthe.2022.05.019

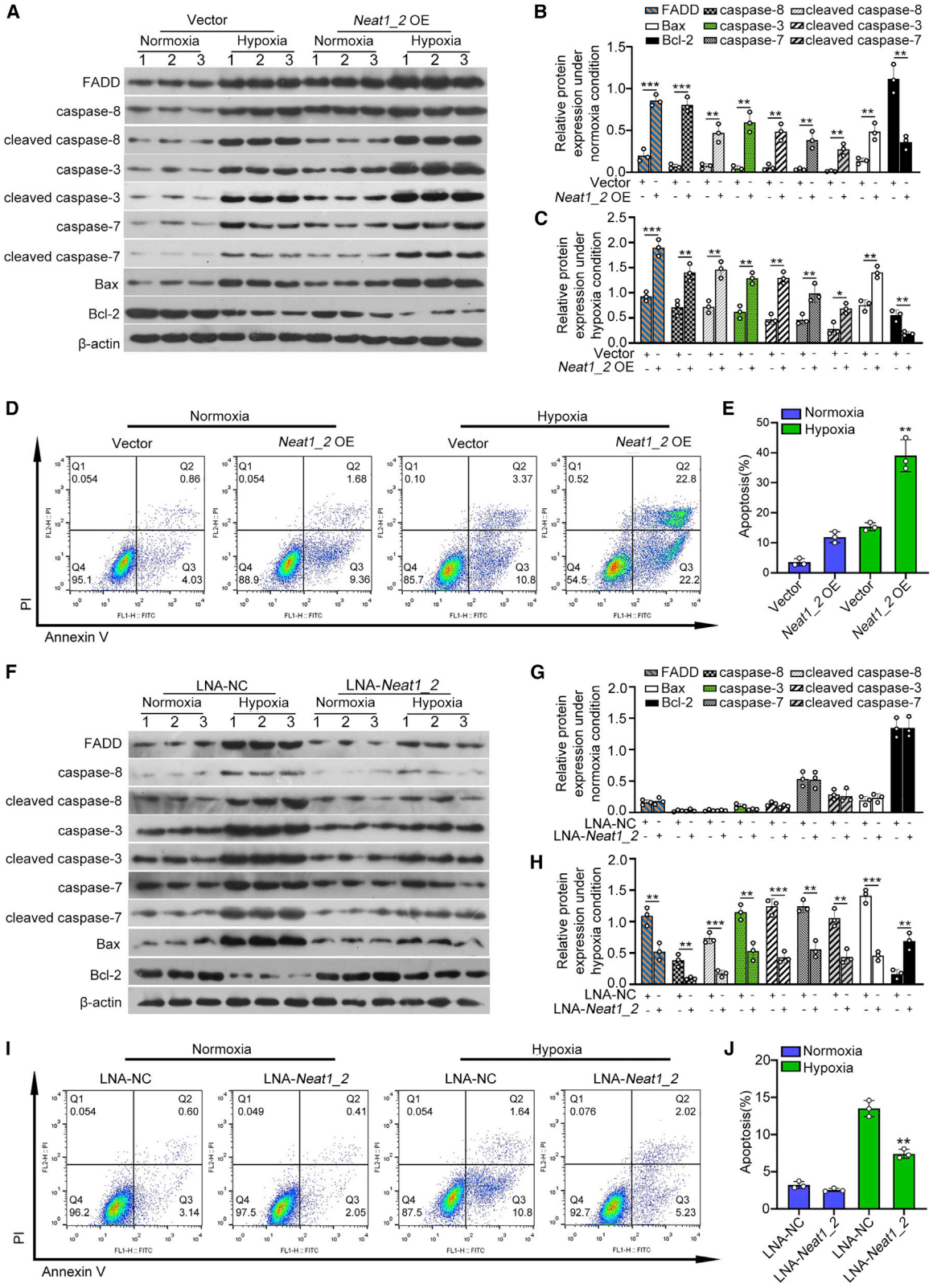

(legend on next page)

Given that *Neat1_2* was significantly upregulated in TECs from severe IRI mice, we hypothesized that *Neat1_2* promoted the apoptosis of TECs during renal IRI. To study the role of *Neat1_2* in TEC apoptosis *in vitro*, TECs were overexpressed with *Neat1_2* in the presence or absence of hypoxia treatment. qPCR showed the overexpression efficacy of *Neat1_2* in TECs (Figures S2E and S2F). Ectopic expression of *Neat1_2* promoted the expression of pro-apoptotic members at both mRNA (Figures S2G–S2J) and protein levels in the presence or absence of hypoxia treatment (Figures 2A–2C). Consistently, overexpression of *Neat1_2* promoted TEC apoptosis under normal or hypoxic conditions (Figures 2D and 2E).

Knockdown of *Neat1_2* was performed by locked nucleic acids (LNAs) to induce RNase-H-mediated degradation. qPCR showed that *Neat1_2* was knocked down efficiently in both the nuclear and cytoplasmic portions of TECs in the presence or absence of hypoxia treatment (Figures S2K and S2L). The expression of apoptosis-associated members was inhibited at both the mRNA and protein levels when *Neat1_2* was knocked down under hypoxic conditions (Figures 2F–2H and S2M–S2P). However, *Neat1_2* knockdown did not have an effect under normoxia conditions. The inhibition of hypoxia-induced TEC apoptosis by *Neat1* knockdown was further verified by annexin V labeling flow cytometry assays (Figures 2I and 2J).

Neat1_2 activates the apoptotic cascade via inhibition of *miR-129-5p*

It has been widely reported that lncRNA may act as a microRNA (miRNA) sponge to promote the expression or translation of downstream targets.[28] Given that *Neat1_2* is released from the nucleus to the cytoplasm during hypoxia treatment and that *Neat1_2* overexpression promotes the mRNA expression of a series of pro-apoptotic members (Figures S2G–S2J), we explored whether *Neat1_2* might also function as the competing endogenous (ceRNA) mechanism to promote TEC apoptosis. To validate this hypothesis, miRNAs that may bind to *Neat1_2* were predicted by the usage of five bioinformatic website tools (AnnoLnc2, ENCORI, RNA22, DIANA, and Starbase).[29,30] Among the candidate miRNAs, 4 miRNAs (*miR-22-3p*, *miR-129-5p*, *miR-194-5p*, and *miR-204-5p*) were predicted by all 5 databases (Figure 3A). To verify the regulatory capability of the miRNAs to *Neat1_2*, we constructed the *Neat1_2* luciferase reporter system. Each predicted miRNA mimics was co-transfected with the *Neat1_2* luciferase reporter into HEK-293T cells. We found that all four miRNAs were able to reduce luciferase activity, and *miR-129-5p* reduced the most, by at least 85% (Figure 3B). Furthermore, *miR-129-5p* expression was markedly reduced in hypoxia-treated TECs, while the expression levels of the other three miRNAs remained constant or upregulated (Figure 3C). Knockdown of *Neat1_2* promoted the expression of *miR-129-5p* in HK2 cells in the presence or absence of hypoxia treatment (Figure 3D). Therefore, *miR-129-5p* was chosen for further study. Ago2 RNA immunoprecipitation (RIP) analysis showed that *Neat1_2* and *miR-129-5p* were significantly enriched in Ago2-containing micro-ribonucleoprotein complexes (Figure 3E), further verifying that *Neat1_2* directly bound to *miR-129-5p* in TECs. RNA FISH showed colocalization of *Neat1_2* with *miR-129-5p* in the cytoplasm of hypoxia-treated HK2 cells (Figure 3F). A pull-down assay with biotinylated *miR-129-5p* was performed to confirm the specific binding between *Neat1_2* and *miR-129-5p* (Figure 3G). To further confirm the association of *Neat1_2* with *miR-129-5p*, we constructed luciferase reporters containing the 5,000- to 6,000-nt sequence of *Neat1_2*, which contained wild-type (WT) or mutated *miR-129-5p* targeting sites (Figure 3H). These reporters were co-transfected with *miR-129-5p* mimics into HEK-293T cells. We found that *miR-129-5p* mimics reduced the reporter activity of the construct with WT *Neat1_2* (Figure 3I). Consistently, hypoxia treatment-induced TEC apoptosis was alleviated by *miR-129-5p* mimics, while cotransfection of *miR-129-5p* mimics with *Neat1_2* plasmids inhibited the antiapoptotic function of *miR-129-5p* mimics (Figures 3J and 3K).

Neat1_2 upregulates the expression of *FADD*, *CASP8*, and *CASP3* via inhibition of *miR-129-5p*

Next, the mechanism by which *Neat1_2* promoted TEC apoptosis was elucidated. Among the predicted targets of *miR-129-5p* by the ENCORI database, *FADD*, *Casp8*, and *Casp3* stood out as attractive candidates because they promoted cell apoptosis and were upregulated in TECs overexpressing *Neat1_2* (Figures 2A–2C). The putative *miR-129-5p*-binding sites in the 3′ UTR of *FADD*, *Casp8*, and *Casp3* are presented in Figure 4A. To verify whether these genes were direct targets of *miR-129-5p*, a dual-luciferase reporter system was used. A firefly luciferase reporter construct containing the WT or mutant 3′ UTR of the target gene was co-transfected with *miR-129-5p* mimics. Luciferase reporter assays showed that the luciferase activities of *FADD*, *Casp8*, and *Casp3* WT reporter were significantly reduced when transfected with *miR-129-5p* mimics compared with mutated reporter (Figures 4B–4D). Furthermore, the overexpression of *miR-129-5p* inhibited the hypoxia-induced increase in pro-apoptotic genes at both mRNA and protein levels (Figures 4E–4G). In the rescue experiments, the overexpression of *miR-129-5p* partly counteracted the corresponding increase in pro-apoptotic genes induced by *Neat1_2* overexpression in TECs (Figures 4H–4J). Furthermore, the luciferase

Figure 2. Upregulation of *Neat1_2* activates TEC apoptosis

(A–C) Representative western blot analyses and quantification data showed cellular expression of pro-apoptotic factors in *Neat1_2*-overexpressed HK2 cells in the presence or absence of hypoxia treatment for 24 h. (D and E) The effect of *Neat1_2* overexpression on apoptosis and the quantification data. Cell apoptosis was assayed by co-staining of annexin V and propidium iodide followed by flow cytometric analysis. (F–H) Representative western blot analyses and quantification data showed cellular expression of pro-apoptotic factors in *Neat1_2*-knocked down HK2 cells in the presence or absence of hypoxia treatment for 24 h. (I and J) The effect of *Neat1_2* knockdown on apoptosis and the quantification data.

The data are presented as means ± SDs. A Student's t test was used for the comparison of 2 groups. ANOVA was used for comparison among multiple groups. $^{*}p < 0.05$, $^{**}p < 0.01$, $^{***}p < 0.001$.

Please cite this article in press as: Ma et al., *Neat1* promotes acute kidney injury to chronic kidney disease by facilitating tubular epithelial cells apoptosis via sequestering *miR-129-5p*, Molecular Therapy (2022), https://doi.org/10.1016/j.ymthe.2022.05.019

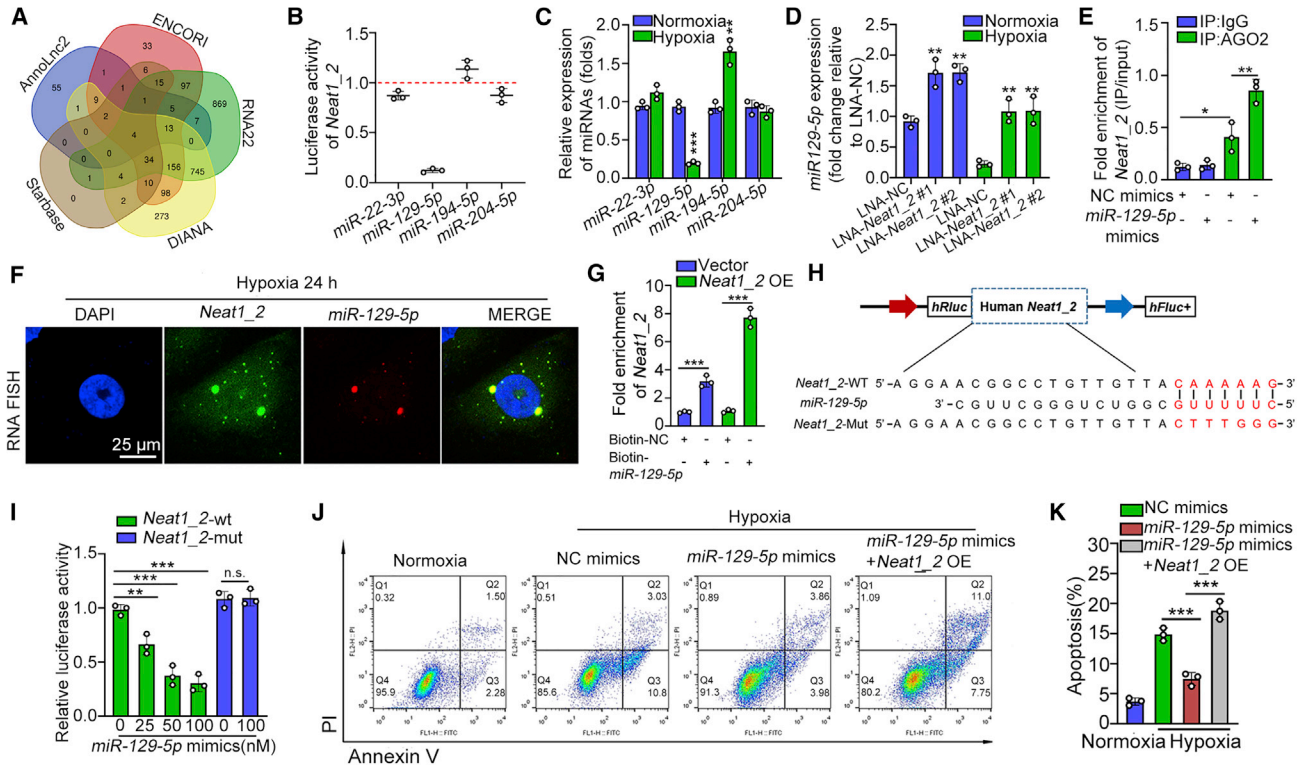

Figure 3. *Neat1_2* activates the apoptotic cascade via inhibition of *miR-129-5p*

(A) Venn diagram of predicted miRNAs interacted with *Neat1_2* in 5 databases. Four miRNAs were the intersection of these databases. (B) Luciferase activity of *Neat1_2* in HEK-293T cells transfected with mimics of miRNAs that putatively bind to the *Neat1_2* sequence. (C) Expression levels of the 4 putative *Neat1_2*-interacting miRNAs in HK2 cells treated with hypoxia for 24 h, assayed by qPCR. (D) Expression of the 4 putative *Neat1_2*-interacting miRNAs in HK2 cells transfected with locked nucleic acid (LNA) targeting *Neat1_2* in the presence or absence of hypoxia treatment, assayed by qPCR. (E) RIP assay were performed using AGO2 antibody in HK2 cells transfected with *miR-129-5p* mimics or mimics negative control (mimic NC), then the enrichment of *Neat1_2* was detected. (F) FISH was performed to observe the cellular location of *Neat1_2* (green) and *miR-129-5p* (red) in HK2 cells treated with hypoxia for 24 h. Scale bar, 25 μm. (G) *Neat1_2* was pulled down and enriched with 3′ end biotinylated *miR-129-5p* in the lysates of HK2 cells transfected with *Neat1_2* overexpression plasmids or empty vector. (H) Schematic illustration of *Neat1_2*-WT and *Neat1_2*-Mut luciferase reporter vectors. (I) Luciferase assays in HEK-293T cells co-transfected with *Neat1_2*-WT or *Neat1_2*-Mut luciferase reporter vectors together with different doses of *miR-129-5p* mimics. (J and K) The effect of *miR-129-5p* mimics on apoptosis in HK2 cells treated with hypoxia for 24 h, in the presence or absence of *Neat1_2* overexpression, and the quantification data. The data are presented as means ± SDs. A Student's t test was used for the comparison of 2 groups. ANOVA was used for comparison among multiple groups. *p < 0.05, **p < 0.01, ***p < 0.001.

activity levels of *FADD*, *Casp8*, and *Casp3* WT reporter were upregulated by *Neat1_2*, while mutations of *miR-129-5p* binding sites in these reporters abrogated the effect of *Neat1_2* (Figure 4K). Consistently, transfection of *miR-129-5p* mimic reduced the TEC apoptosis induced by *Neat1_2* overexpression (Figures 4L and 4M). To exclude that *miR-129-5p* directly inhibits *Casp-7* and *Bax* expression, firefly luciferase reporter containing 3′ UTR of *Casp-7* and *Bax* was separately co-transfected with *miR-129-5p* mimics. The results showed that *miR-129-5p* mimics had no effect on the luciferase activity of *Casp-7* and *Bax* (Figures 4N and 4O). To explore the underlying mechanism for the inhibition effect of *miR-129-5p* on caspase-7 and Bax, we found that the knockdown of *FADD* was able to counteract the upregulation of caspase-7 and Bax triggered by *miR-129-5p* inhibition (Figures 4P and 4Q). These data suggested that *Neat1_2* promoted *FADD*, *Casp8*, and *Casp3* expression and subsequent apoptosis by sequestering *miR-129-5p*.

Knockdown of endogenous *Neat1_2* protects against AKI after IRI by inhibiting TEC apoptosis

To explore the role of *Neat1_2* in promoting AKI-to-CKD transition, we verified the expression of apoptosis-related parameters, profibrotic genes, *Neat1_2*, and *miR-129-5p* in the course of the AKI-to-CKD transition. The results showed that the expression of *Neat1_2* increased 1 day post-I/R injury and lasted until 28 days after injury, accompanied by an increase in the expression of p53, FADD, caspase-3, caspase-8, and collagen I. Moreover, we observed a decreased expression in *miR-129-5p* 1 day post-injury and lasted until 28 days after injury (Figures S3A–S3D).

To investigate the function of *Neat1_2* in this model, we knocked down renal *Neat1_2* expression *in vivo* by adeno-associated virus serotype 9 (AAV9) harboring small interfering RNA (siRNA) sequence targeting *Neat1_2* (termed AAV9-si*Neat1_2*). Twenty-one

Please cite this article in press as: Ma et al., *Neat1* promotes acute kidney injury to chronic kidney disease by facilitating tubular epithelial cells apoptosis via sequestering *miR-129-5p*, Molecular Therapy (2022), https://doi.org/10.1016/j.ymthe.2022.05.019

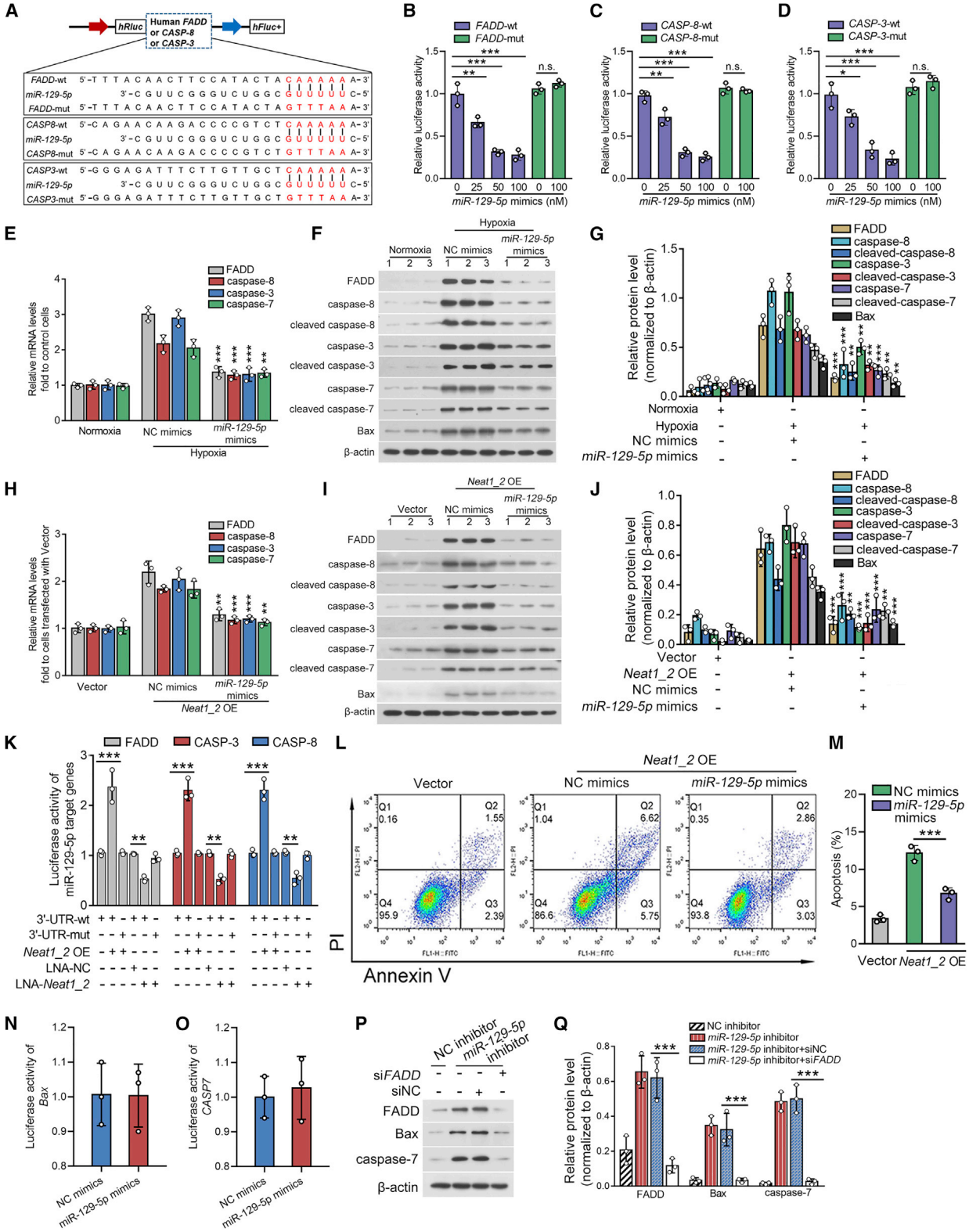

(legend on next page)

days after injection, mice were subjected to 40 min of IRI and were sacrificed at 24 h after surgery (Figure 5A). The infection rate of AAV is >70% of the tubular cells in the renal cortex (Figures S3E and S3F). ISH and qPCR in renal tissue showed the efficacy of *Neat1_2* knockdown (Figures 5B–5D). We further found a noticeable increase in the expression of *miR-129p* in the renal cortex from IRI mice delivered with AAV9-si*Neat1_2*, as compared to IRI mice delivered with negative control (Figure 5E). To examine the outcome of *Neat1_2* depletion in AKI, we further examined renal histological injury and quantified the acute tubular injury score after periodic acid-Schiff (PAS) staining, and the results showed that tubular injury was ameliorated by *Neat1_2* knockdown (Figures 5F and 5G). As shown in Figure 5H, serum creatinine levels revealed that *Neat1_2* depletion improved renal function in IRI-treated mice. To quantitatively evaluate TEC apoptosis, apoptotic cells accessed by TUNEL staining were evaluated. The results showed that the knockdown of *Neat1_2* decreased tubular cell apoptosis in IRI-treated mice (Figures 5I and 5J). Consistently, depletion of *Neat1_2* decreased the mRNA and protein levels of pro-apoptotic factors (Figures 5K–5O).

Since *Neat1_2* is highly conservative within the mammalian lineage,[31] suggesting critical function for this lncRNA. To explore whether *Neat1_2* may function in another AKI model, the effect of *Neat1_2* was studied in cisplatin-induced AKI. The results showed that *Neat1_2* was effectively knocked down while the downregulation of *miR-129-5p* was partly prevented (Figures S3G and S3H). The cisplatin-induced AKI was ameliorated, as shown by the decrease of AKI score and serum creatinine (Figures S3I–S3K). Moreover, depletion of *Neat1_2* inhibited TEC apoptosis in cisplatin-treated mice (Figures S3L–S3O).

Expression of exogenous *Neat1_2* aggravates AKI after IRI

To further verify the effect of *Neat1_2* on AKI, AAV9 harboring empty vector (called AAV9-Vector) or *Neat1_2* full length (called AAV9-*Neat1_2*) was injected into the renal vein, respectively, 3 weeks before IRI treatment. Mice were sacrificed 1 day after surgery (Figure 6A). The renal expression of *Neat1_2* in mice delivered with AAV9-*Neat1_2* was increased at 24 h after IRI treatment, accompanied by the further decrease in *miR-129-5p*, as compared to their littermate control treated with AAV9-Vector (Figures 6B–6E). The overexpression of exogenous *Neat1_2* further elevated serum creatinine levels (Figure 6F), exacerbated tubule injury (Figures 6G and 6H), and promoted TEC apoptosis 1 day post-IRI (Figures 6I and 6J). Furthermore, ectopic expression of *Neat1_2* increased the mRNA and protein levels of pro-apoptotic factors (Figures 6K–6O).

Inhibition of *Neat1_2* preserves tubular integrity and improves tubulointerstitial fibrosis by elevating *miR-129-5p* expression

To validate the role of *Neat1_2*-induced TEC apoptosis in mediating AKI-CKD progression, mice were treated with AAV9-si*Neat1_2* or AAV9-*Neat1_2* to knockdown or overexpress *Neat1_2*, respectively. Mice were sacrificed at 11 days after surgery (Figure 7A). The assessment of *Neat1_2* and *miR-129-5p* expression was carried out in renal tissue and the results showed that *Neat1_2* was effectively knocked down in mice treated with AAV9-si*Neat1_2*, with an increase in *miR-129-5p* expression (Figures S4A and S4B). Consistent with these results, *miR-129-5p* expression was further reduced in *Neat1_2*-overexpressed mice (Figures S4C and S4D). Depletion of *Neat1_2* ameliorated IRI-induced renal fibrosis (Figures 7B and 7C), reduced renal inflammation (Figures 7D–7F), decreased TEC apoptosis (Figures 7G–7J), preserved tubular integrity (Figures 7K and 7L), and decreased the expression of the extracellular matrix (Figures 7M–7P). In contrast, ectopic expression of *Neat1_2* further increased renal inflammation (Figures S4E–S4G), exacerbated renal fibrosis (Figures S4H and S4I), promoted TEC apoptosis (Figures S4J–S4M), and enhanced the expression of the extracellular matrix (Figures S4N–S4Q).

To exclude that the ameliorative effect of *Neat1_2* knockdown on the chronic progression of AKI may be due to its protective efficacy on the acute injury, the IRI mice were treated with *Neat1_2* knockdown 4 days after IRI treatment. Then, mice were sacrificed 28 days after IRI treatment. The depletion of *Neat1_2* was also found to inhibit severe renal fibrosis that developed in mice at day 28 after IRI, which was proved by the reduced tubulointerstitial fibrosis (TIF) index (Figures 7Q and 7R) and decreased expression of extracellular matrix (Figures 7S and 7T).

To test the involvement of *miR-129-5p* in renal fibrosis, we explored the effect of anti-*miR-129-5p in vivo* by injecting anti-*miR-129-5p* LNA or scrambled sequence LNA in AAV9-si*Neat1_2*-treated IRI mice. The results showed that *miR-129-5p* expression was substantially inhibited by anti-*miR-129-5p* LNA (Figure S5A) and that

Figure 4. *miR-129-5p* inhibits *Neat1_2*-mediated TEC apoptosis *in vitro* through targeting the 3′ UTR of *FADD*, *CASP-3*, and *CASP-8*

(A) Schematic illustration of *FADD*-WT, *CASP-8*-WT, *CASP-3*-WT, *FADD*-Mut, *CASP-8*-Mut, and *CASP-3*-Mut luciferase reporter vectors. (B-D) Luciferase assays in HEK-293T cells co-transfected with WT or mutated luciferase reporter vectors of *FADD* (B), *CASP-8* (C), and *CASP-3* (D), together with different doses of *miR-129-5p* mimics. (E) qPCR showing the expression of pro-apoptotic factors in HK2 cells transfected with mimic NC or *miR-129-5p* under hypoxia treatment for 24 h. (F and G) Western blot showing the expression of pro-apoptotic factors in HK2 cells transfected with mimic NC or *miR-129-5p* under hypoxia treatment for 24 h. (H) qPCR showing the expression of pro-apoptotic factors in *Neat1_2*-overexpressed HK2 cells transfected with mimic NC or *miR-129-5p*. (I and J) Western blot showing the expression of pro-apoptotic factors in *Neat1_2*-overexpressed HK2 cells transfected with mimic NC or *miR-129-5p*. (K) Luciferase assays in HK2 cells co-transfected with WT or mutated luciferase reporter vectors of *FADD*, *CASP-8*, and *CASP-3*, together with *Neat1_2* depletion or overexpression. (L and M) The effects of *miR-129-5p* mimics on apoptosis in HK2 cells induced by *Neat1_2* overexpression, and the quantification data. (N and O) Luciferase assays in HK2 cells co-transfected with luciferase reporter vectors of *Bax* and *CASP-7* together with *Neat1_2* overexpression. (P and Q) Western blot showing the expression of FADD, Bax, and caspase-7 in *miR-129-5p* inhibitor-transfected HK2 cells, together with *FADD* or scramble siRNAs transfection. The data are presented as means ± SDs. A Student's t test was used for the comparison of 2 groups. ANOVA was used for comparison among multiple groups. *$p < 0.05$, **$p < 0.01$, ***$p < 0.001$.

Please cite this article in press as: Ma et al., *Neat1* promotes acute kidney injury to chronic kidney disease by facilitating tubular epithelial cells apoptosis via sequestering *miR-129-5p*, Molecular Therapy (2022), https://doi.org/10.1016/j.ymthe.2022.05.019

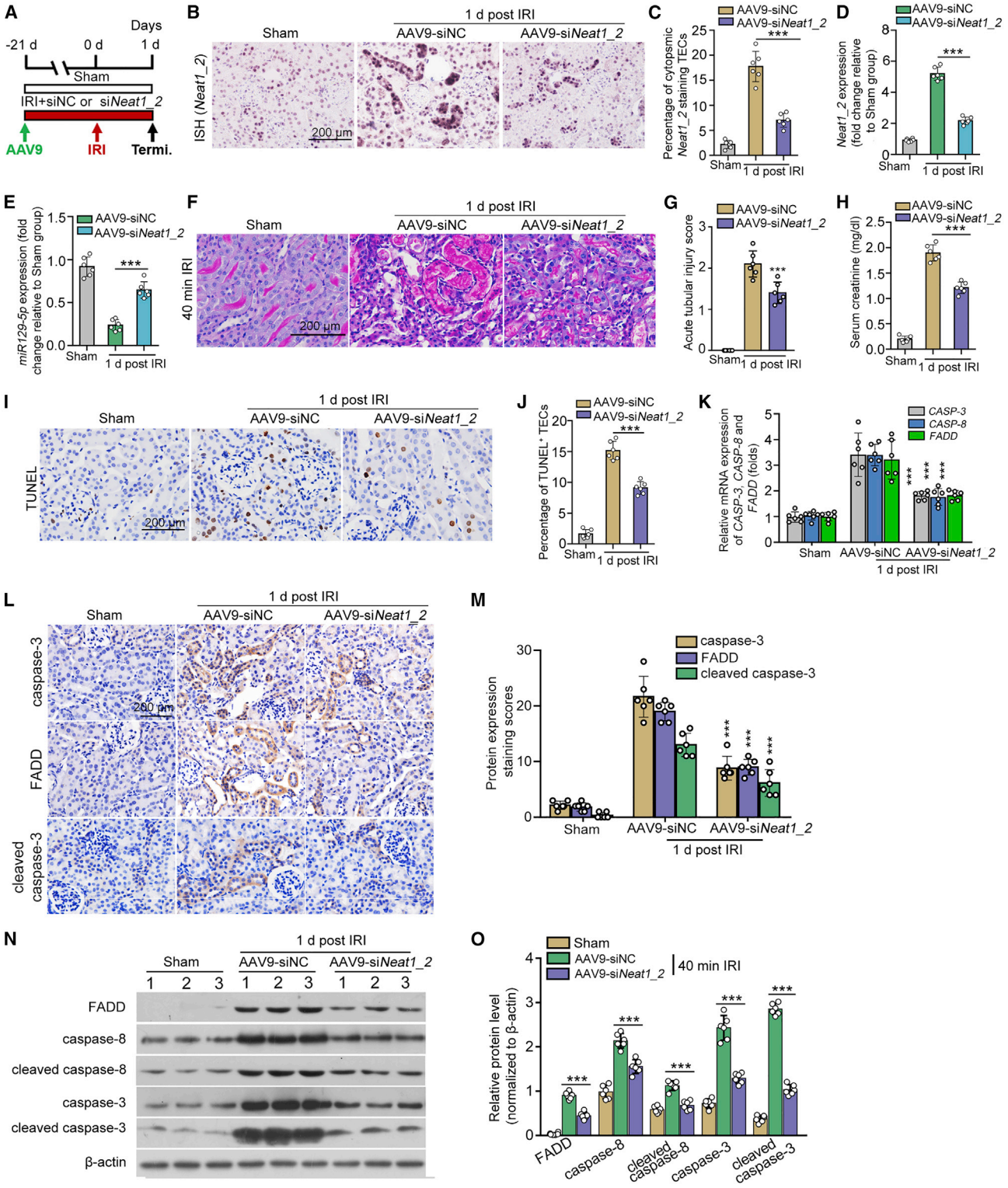

Figure 5. Knockdown of endogenous *Neat1_2* protects against AKI after IRI by inhibiting TECs apoptosis

(A) Mice were treated by renal vein injection of either AAV9-si*Neat1_2* or AAV9-siNC 21 days before establishing IRI. (B and C). Representative images of ISH of *Neat1_2* expression in kidneys from IRI mice injected with AAV9-si*Neat1_2* (B) and the percentage of cytoplasmic *Neat1_2* positive TECs (C). (D and E) qPCR showing the expression

(legend continued on next page)

Please cite this article in press as: Ma et al., *Neat1* promotes acute kidney injury to chronic kidney disease by facilitating tubular epithelial cells apoptosis via sequestering *miR-129-5p*, Molecular Therapy (2022), https://doi.org/10.1016/j.ymthe.2022.05.019

miR-129-5p inhibition was able to counteract the decrease in TIF score (Figures S5B and S5C), triggered by *Neat1_2* silencing, increasing the expression of profibrotic proteins, as compared with AAV9-si*Neat1_2* treated IRI mice injected with scrambled sequence LNA (Figures S5D and S5E).

Neat1_2 upregulation associates with epithelial cell apoptosis in human AKI

To evaluate the role of *Neat1_2* in the pathogenesis of human AKI, we conducted a cross-sectional analysis for the association of *Neat1_2* expression and the apoptosis-related parameters in a cohort of 15 patients with biopsy-proven AKI. The characteristics of patients at the time of biopsy are shown in Table S4. ISH showed that *Neat1_2* was expressed mainly in the nucleus of TECs of normal kidneys (Figure 8A). The expression level of *Neat1_2* was remarkably elevated, and cytoplasmic translocation of *Neat1_2* was observed in renal biopsy samples from patients with AKI, accompanied by enhanced TEC apoptosis, which was reflected by the increase in $TUNEL^+$ TECs and pro-apoptotic protein expression (Figures 8A–8G). Correlation analysis showed positive correlations between intrarenal expression of *Neat1_2* and acute tubular injury score or $TUNEL^+$ TECs accumulation (Figures 8H and 8I).

DISCUSSION

After AKI, the kidney sometimes completely recovers its function and structure by an adaptive repair with the regeneration of TECs or undergoes maladaptive responses under other conditions, leading to the progression of fibrotic CKD.[32] Whether lncRNAs govern such distinct outcomes of AKI remains largely unclear. In this study, we screened for differentially expressed lncRNAs in isolated tubules from mild and severe IRI mouse kidneys. We demonstrated the molecular mechanisms of *Neat1_2* underlying the divergent fates of the kidneys after AKI. Our results show that *Neat1_2* upregulation plays a crucial role in driving CKD progression after severe IRI. This conclusion is supported by several lines of evidence, which include (1) aberrant upregulation and cytoplasmic translocation of *Neat1_2* observed 1 through 42 days post-severe IRI, but not mild IRI, are associated with developing CKD after severe AKI; (2) TEC apoptosis is dramatically increased in mice with severe renal IRI, and overexpression of *Neat1_2* leads to TEC apoptosis *in vitro*; (3) ectopic expression of *Neat1_2* accelerates CKD progression *in vivo* by promoting kidney injury and TEC apoptosis; and (4) depletion of *Neat1_2* with AAV9 carrying siRNAs in mouse kidney reduces renal injury and inflammation, prevents AKI-CKD progression, and ameliorates renal fibrosis. Collectively, these findings establish a critical role for aberrant *Neat1_2* expression in driving AKI to CKD progression.

It is generally recognized that the ultimate outcomes of patients who survive an episode of AKI are divergent. Although some patients with AKI may have a better prognosis with complete restorations of renal function and structure, others unfortunately will progress to CKD with declining renal function and will develop renal fibrosis. Although many host factors, such as preexisting conditions and hereditary information, have roles in this process, the severity of AKI seems to be the most critical predictor of poorer outcomes.[33,34] The mouse model of bilateral IRI, which we applied in this study, is a well-established model of AKI.[35] Consistent with the clinical findings, the results of the IRI mouse model showed that in mice with identical age, gender, and genetic background, the severity of renal ischemia per se is the single most important element for determining the ultimate outcome of AKI. We found that a 40-min IRI resulted in severe AKI followed by progression to CKD, whereas a 20-min IRI triggered transient AKI followed by renal recovery (Figures S1A–S1G). Therefore, by merely altering the duration of ischemia, one can establish both models of severe AKI destined for progressive CKD and mild AKI with complete recovery in the same setting. Such IRI models with divergent renal outcomes provide an incomparable tool for screening lncRNAs that regulate AKI to CKD progression after severe AKI. Intriguingly, the *Neat1_2* RNA transcript is evolutionarily conserved at the nucleotide level in humans and mice. Hence, findings in mice may be translated into improvements in diagnosis and therapy of patients. Patients at high risk of renal I/R injury may greatly benefit from *Neat1_2* inhibition before a procedure.

Our studies also provide evidence that TEC apoptosis of varying degrees of severity controls the different long-term outcomes of AKI. AKI is characterized by tubular cell apoptosis and renal inflammation, followed by the proliferation of the remaining tubular cells, leading to recovery or progression to CKD.[21,36] By unbiased mRNA-seq followed by bioinformatics analysis between the isolated tubules from mild and severe IRI kidney, the mRNAs regulating the apoptotic process were found to be significantly altered in severe IRI kidneys (Figures S2A and S2B). These results showed that the increased apoptotic TECs may greatly contribute to AKI-CKD progression. Indeed, we found that *Neat1_2* promoted the progression of AKI to CKD by simultaneously upregulating the expression levels of the pro-apoptotic factors FADD, caspase-3, and caspase-8 via sequestering *miR-129-5p* (Figure 8J). According to our results, *miR-129-5p* decreased both the total and cleaved form of caspase-3

of *Neat1_2* (D) and *miR-129-5p* (E) in renal cortex from IRI mice treated with AAV9-si*Neat1_2*. (F and G) Representative micrographs showing kidney injury in different groups 1 day after IRI injury (F), and the quantification data of acute tubular injury score (G). (H) Serum creatinine level in IRI mice injected with either AAV9-si*Neat1_2* or AAV9-siNC 1 day post IRI. (I and J) Representative images of TUNEL staining showing a reduced percentage of TECs apoptosis in the kidneys from IRI mice injected with AAV9-si-*Neat1_2* (I), and the quantification data (J). (K) qPCR showed that depletion of *Neat1_2* decreased the mRNA expression of pro-apoptotic factors in renal cortex homogenates from mice subjected to IRI. (L and M) Representative immunohistochemistry images showing the expression levels of pro-apoptotic factors in IRI mice injected with either AAV9-si*Neat1_2* or AAV9-siNC 1 day post IRI (L), and the quantification data (M). (N and O) Western blot showed that depletion of *Neat1_2* decreased the protein expression of pro-apoptotic factors in renal cortex homogenates from mice subjected to IRI. Scale bars in (B), (F), (I), (L) are 200 μm. The data are presented as means ± SDs. A Student's t test was used for the comparison of 2 groups. ANOVA was used for comparison among multiple groups (n = 6 for each group). ***$p < 0.001$.

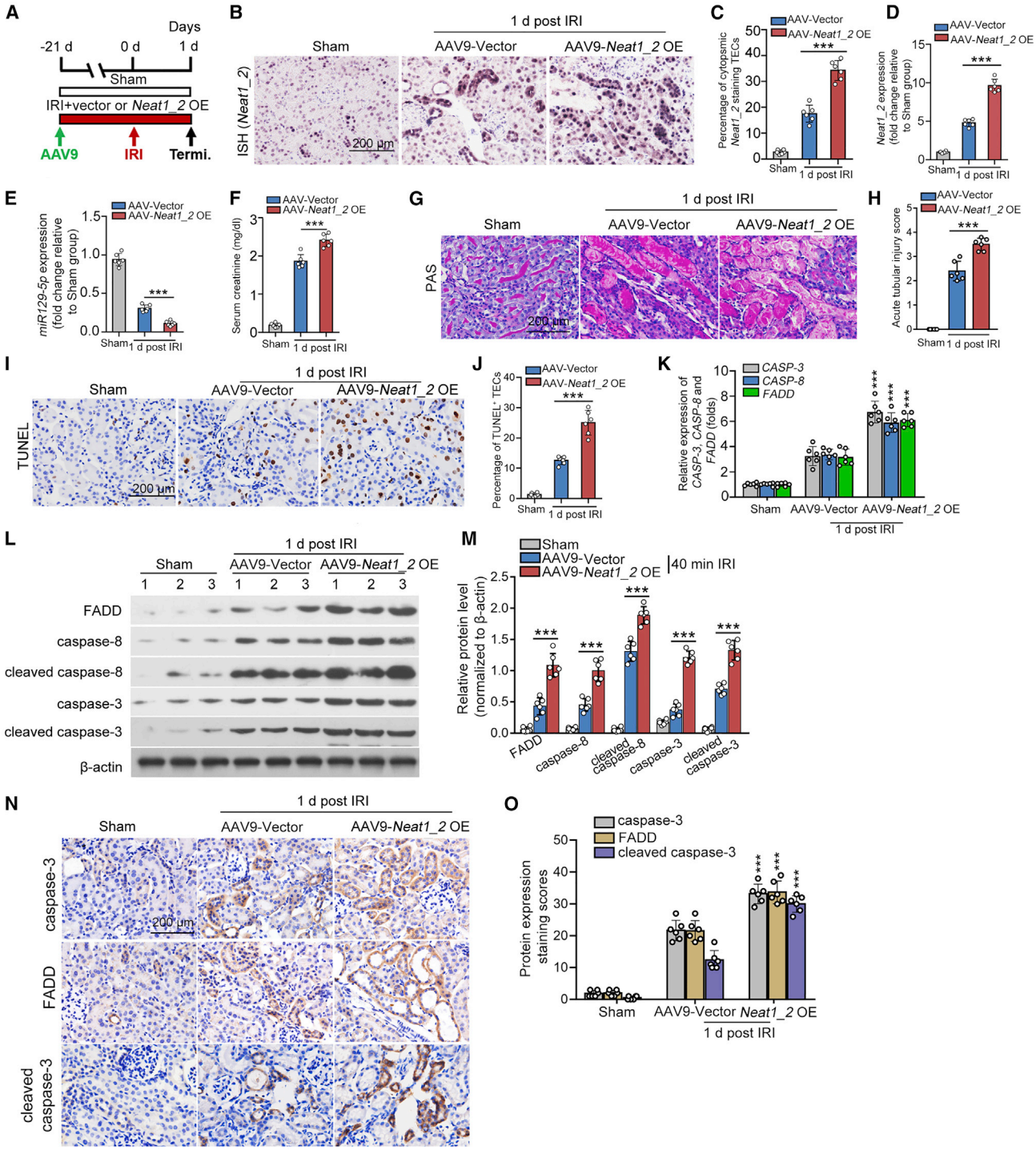

Figure 6. Expression of exogenous *Neat1_2* aggravates AKI after IRI

(A) Mice were treated by renal vein injection of either AAV9-Vector or AAV9-*Neat1_2* 21 days before performing IRI. (B and C) Representative images of ISH of *Neat1_2* expression in kidneys from IRI mice injected with AAV9-*Neat1_2* (B) and the percentage of cytoplasmic *Neat1_2* positive TECs (C). (D and E) qPCR showing the expression of *Neat1_2* (D) and *miR-129-5p* (E) in renal cortex from IRI mice treated with AAV9-*Neat1_2*. (F) Serum creatinine level in IRI mice injected with either AAV9-Vector or AAV9-*Neat1_2* 1 day post IRI. (G and H) Representative images showing kidney injury in different groups 1 day after IRI injury (G), and the quantification data of acute kidney injury score (H). (I and J) Representative images of TUNEL staining showing an increased TECs apoptosis in the kidneys from IRI mice injected with AAV9-*Neat1_2* (I), and the

(legend continued on next page)

and caspase-8, suggesting that miRNA may decrease both the total and cleaved forms of these caspase members. This is not an exception—for example, *miR-221* could decrease both the total and cleaved forms of caspase-3 in hepatocellular carcinoma cells.[37]

Interestingly, *Neat1* was originally characterized as a lncRNA with abundant nuclear expression.[38] In this study, by several techniques, we found that *Neat1_2* transcript was dramatically increased in the cytoplasm of TECs in severe IRI mice and renal biopsy samples from AKI patients, indicating that *Neat1_2* may function in the cytoplasm during TEC injury. These results further supported our findings that *Neat1_2* sponged *miR-129-5p* to upregulate the expression of pro-apoptotic genes.

Previous studies have shown that *Neat1* is a critical lncRNA involved in AKI development. *Neat1* promoted lipopolysaccharide (LPS)-induced TECs injury and inflammation by elevating the expression of TRAF6.[39] Knockdown of *Neat1* promoted macrophage M2 polarization under LPS treatment *in vitro*, ameliorating the inflammatory responses by *miR-125-5p*/TRAF6/TAK1 axis.[40] Moreover, *Neat1* was also proved to aggravate renal fibrosis in a mouse unilateral ureteral obstruction model and a mouse diabetic nephropathy model. *Neat1* was proved to aggravate renal fibrosis by promoting the expression of collagen I by sequestering *miR-129*[41] or activating ERK1/2 and Akt/mTOR signaling[42,43] separately. In our study, *Neat1_2* was upregulated in TECs from mice with severe AKI, suggesting that *Neat1_2* may regulate the AKI to CKD progression. Indeed, by gain- and loss-of-function studies *in vivo*, we found that *Neat1_2* promoted renal fibrosis post-IRI-induced AKI via a *miR-129-5p*/FADD/caspase-8/caspase-3 axis.

It has been demonstrated that *p53* promoted the apoptosis of TECs during AKI.[44] In this study, we screened for the transcriptional factor governing *Neat1_2* upregulation in injured TECs and found that p53 controlled *Neat1_2* expression by directly binding to the promoter of *Neat1_2* under hypoxia treatment, thereby upregulating the expression of *Neat1_2* in TECs.

In conclusion, for the first time, our study identified a highly conserved and pro-apoptotic lncRNA that promoted AKI-CKD progression. These findings provide novel information for understanding the mechanism underlying TEC apoptosis in severe ischemia-induced AKI. Our work hints at the possibility of a new therapeutic target to halt AKI-CKD progression.

MATERIALS AND METHODS

Cell culture and hypoxia treatment

Human TEC HK2 (American Type Culture Collection [ATCC], Manassas, VA, USA) were commercially available. The immortalized mTECs were a gift from H.-Y. Lan (The Chinese University of Hong Kong). Cells were cultured in Dulbecco's modified Eagle's medium (DMEM)/Ham's F12 medium (Invitrogen, Grand Island, NY, USA) supplemented with 10% fetal bovine serum (Invitrogen). Human embryonic kidney 293T (HEK293T) cells (ATCC) were cultured in DMEM (Invitrogen) supplemented with 10% fetal bovine serum. These cells were maintained at 37°C in an atmosphere containing 5% CO_2. To establish the hypoxia model, human and mouse TECs were deprived of serum overnight when they reached approximately 70% confluence. Then, the cells were incubated in DMEM/Ham's F12 medium at 37°C for the indicated time points in a hypoxia chamber (1% O_2, 5% CO_2, 94% N_2). These cells were further cultured in normal culture medium with constant oxygen for 6 h.

Cell transfection

Overexpression of Neat1_2

The full-length sequence of *Neat1_2* was cloned into pcDNA3.1 (Invitrogen). The cells were transfected with empty vector or the *Neat1_2*-overexpression plasmids for the indicated time points, and then the cells were collected to study the function of *Neat1_2*.

RNA interference for *p53* and *Rela*

For transient transfection, 50%–80% confluent cells were transfected with the siRNAs using Lipofectamine 2000 (Invitrogen) according to the manufacturer's instructions. The sequences of siRNAs are listed in Table S3.

LNA-induced *Neat1_2* knockdown

For *Neat1_2* knockdown experiments, cells were transiently transfected with LNAs antisense oligonucleotides (Exiqon, Vedbaek, Denmark) using Lipofectamine 2000 (Invitrogen) according to the manufacturer's protocol. The LNA sequences are listed in Table S3.

miRNA mimics and miRNA inhibitor

The mimics of *miR-129-5p*, *miR-22-3p*, *miR-194-5p*, and *miR-204-5p* were synthesized by Genepharma (Shanghai, China). The *miR-129-5p* inhibitor used *in vitro* was synthesized by Genepharma. Cells were transfected with miRNA mimics or miRNA inhibitor using Lipofectamine 2000 (Invitrogen).

RNA extraction and qPCR

TRIzol reagent (Thermo Fisher Scientific, Waltham, MA, USA) was used to isolate total RNA from tissues or cells following the manufacturer's instructions. The purity and integrity of the total RNAs were measured by Nanodrop (Thermo Fisher Scientific).

To determine the expression levels of mRNA and lncRNA, first-strand cDNA was prepared using the HiScript III 1st Strand cDNA

quantification data (J). (K) qPCR showed that ectopic expression of *Neat1_2* further increased the mRNA expression of pro-apoptotic factors in kidney homogenates from mice subjected to IRI. (L and M) Western blot showed that overexpression of *Neat1_2* in IRI mice further promoted the expression of pro-apoptotic factors in kidney homogenates from mice subjected to IRI. (N and O) Representative images of immunohistochemistry showed that overexpression of *Neat1_2* in IRI mice further promoted the expression of pro-apoptotic factors. Scale bars in (B), (G), (I), (N) are 200 μm. The data are presented as means ± SDs. A Student's t test was used for the comparison of 2 groups. ANOVA was used for comparison among multiple groups (n = 6 for each group). ***$p < 0.001$.

Please cite this article in press as: Ma et al., *Neat1* promotes acute kidney injury to chronic kidney disease by facilitating tubular epithelial cells apoptosis via sequestering *miR-129-5p*, Molecular Therapy (2022), https://doi.org/10.1016/j.ymthe.2022.05.019

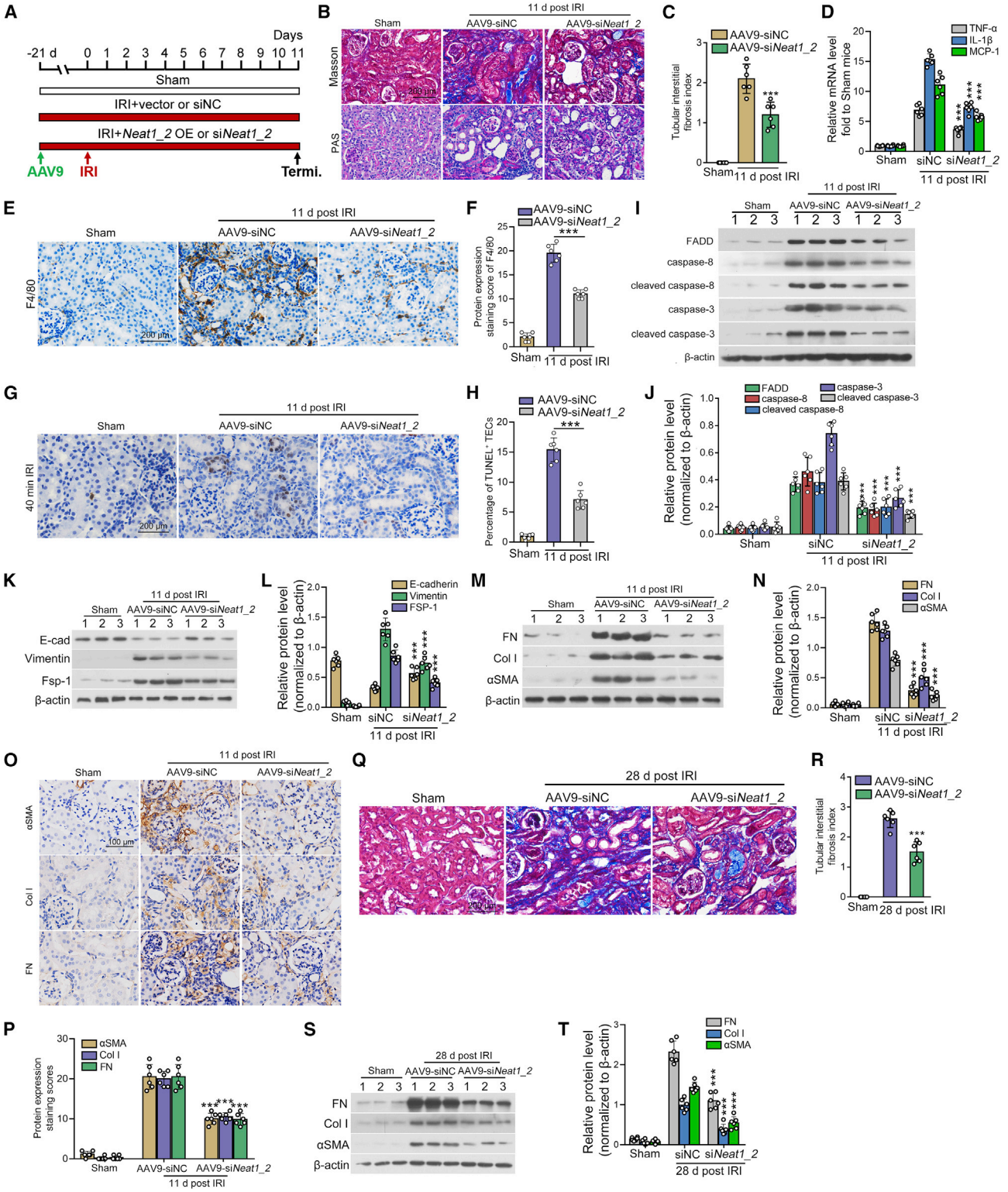

Figure 7. Inhibition of *Neat1_2* preserves tubular integrity and improves tubulointerstitial fibrosis

(A) Mice were treated by renal vein injection of AAV9 to manipulate the expression of *Neat1_2* in mouse kidney 21 days before performing IRI. Mice were sacrificed 11 days post-injury. (B and C) Representative images of Masson's trichrome staining in mice treated with either AAV9-si*Neat1_2* or AAV9-siNC (B), and the quantification data (C).

(legend continued on next page)

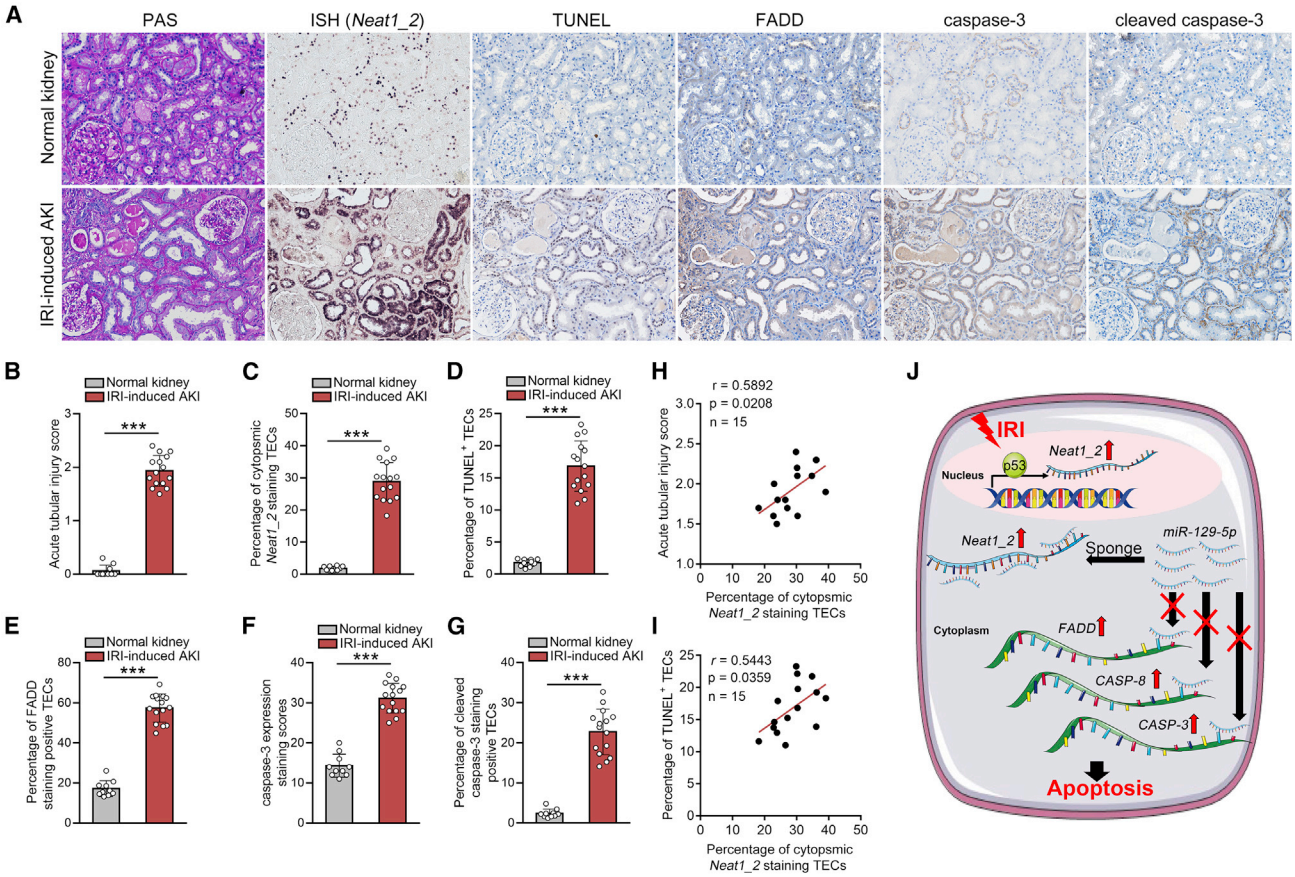

Figure 8. *Neat1_2* upregulation correlates with epithelial cell apoptosis in human AKI

(A–G) Representative images of ISH for *Neat1_2* and TUNEL staining and immunohistochemistry for pro-apoptotic factors in human kidney sections from patients with AKI (A) and quantification data (n = 10 for control, n = 15 for patients with AKI) (B–G). Scale bar in (A) is 200 μm. (H and I) Correlation between *Neat1_2* expression and acute tubular injury score (H), or percentage of TUNEL staining positive TECs (I). (J) Graphical abstract of this study. The data are presented as means ± SDs. In (A)–(G), p values were calculated by Student's t test. In (H) and (I), p values were calculated by Pearson correlation analysis.

Synthesis Kit (Vazyme, Nanjing, China). The qPCR was performed using the Taq Pro Universal SYBR qPCR Master Mix (Vazyme) on a 7500 Fast Real-Time PCR System (Applied Biosystems, Waltham, MA, USA). All of the reactions were performed in triplicate. The sequences of the primer pairs are listed in Table S3.

To determine the expression levels of miRNA, a Mir-X miRNA First-Strand Synthesis Kit (Takara Bio, Kusatsu, Japan) was used according to the manufacturer's instructions. U6 was used as the internal control. For relative miRNA expression, miRNA expression was calculated as $2^{-\Delta CT}$ ($\Delta CT = CT_{miR} - CT_{U6}$).

To determine the cellular location of *Neat1_2*, the nuclear and cytoplasmic fractions of HK2 cells were isolated with PARIS Kit according to the manufacturer's instructions (Thermo Fisher Scientific, Waltham, MA, USA). Total RNA extraction

(D) qPCR showed that depletion of *Neat1_2* decreased the mRNA expression of pro-inflammatory factors in kidney *homogenates* from mice subjected to IRI. (E and F) Representative images of immunohistochemical staining of F4/80 in kidney tissue from mice treated with either AAV9-si*Neat1_2* or AAV9-siNC 11 days post-injury. (G and H) Representative images and quantification data of TUNEL staining showed that depletion of *Neat1_2* inhibited TEC apoptosis. (I and J) Western blot showed that depletion of *Neat1_2* in IRI mice alleviated the expression of pro-apoptotic factors in kidney homogenates from mice subjected to IRI 11 days post-injury. (K and L) Western blot showed that depletion of *Neat1_2* in IRI mice preserved tubular integrity, as reflected by the increase in E-cadherin and decrease in vimentin and FSP-1. (M and N) Western blot showed that inhibition of *Neat1_2* expression decreased the expression of profibrotic factors 11 days post-IRI. (O and P) Immunohistochemical staining of profibrotic factors in kidney tissue from mice treated with either AAV9-si*Neat1_2* or AAV9-siNC 11 days post-injury. (Q and R) Representative images and quantification data of Masson's trichrome staining in IRI mice injected with either AAV9-siNC or AAV9-*siNeat1_2* 28 days post-IRI treatment. (S and T) Western blot showed that inhibition of *Neat1_2* expression decreased the expression of profibrotic factors 28 days post-IRI. Scale bars in (B), (E), (G), (Q) are 200 μm. Scale bar in (O) is 100 μm. The data are presented as means ± SDs. A Student's t test was used for the comparison of 2 groups. ANOVA was used for comparison among multiple groups (n = 6 for each group). ***p < 0.001.

and qPCR were conducted in nuclear and cytoplasmic fractions separately.

Animals and AKI models

All of the animal experiments were approved by the Animal Research Committee of Southern Medical University and performed in accordance with the National Institutes of Health Guide for the Care and Use of Laboratory Animals. The mice were provided by Guangdong Medical Animal Center and housed in cages with free access to water and food in a temperature-controlled room (22°C ± 2°C). Six- to 8-week-old C57BL/6 mice with body weights of 20–24 g were used for the I/R model and cisplatin-induced AKI model. Bilateral renal I/R injury was performed as previously described.[45] Briefly, under general anesthesia by sodium pentobarbital, the bilateral renal pedicles were clipped for 20 or 40 min using microaneurysm clamps (Fine Science Tools, North Vancouver, Canada). After removal of the clamps, reperfusion of the kidneys was visually confirmed. A temperature-controlled heating device was used to maintain the body temperature of the mice between 37°C and 38°C. Sham-operated mice were used as controls.

For cisplatin-induced AKI, mice were subjected to a single i.p. injection of cisplatin (Sigma, St. Louis, MO, USA) at a dose of 40 mg/kg. Mice were sacrificed at day 3 after cisplatin administration.

To explore the regulative effect of p53 on *Neat1_2* expression, mice were subjected to the p53 inhibitor PIF-α[27] by i.p. injection of 2.2 mg/kg PIF-α (Selleckchem, Houston, TX, USA) 12 h before AKI induction, whereas mice in the control group were injected with equivalent PBS.

Renal tubules isolation

To isolate tubules from sham mice and IRI mice, animals were anesthetized at the indicated time points post-surgery. Kidneys were peeled off and the renal cortex was dissected gently and digested in 1 mg/mL collagenase type IV (Thermo Fisher Scientific) for 30 min at 37°C, and then they were resuspended and washed twice with cold PBS. The tubules were isolated using 31% Percoll gradients (General Electric, Boston, MA, USA), then resuspended, and washed with cold PBS. Total RNAs of the collected tubules were extracted with TRIZOL reagent (Invitrogen).

IRI induced AKI-to-CKD model

According to the previous studies, clamping of the renal pedicle for an ischemic duration $\geq$30 min will cause progressive CKD.[6,22] We established the IRI induced AKI-to-CKD model by performing 40-min bilateral renal IRI. Briefly, under general anesthesia, the bilateral renal pedicles were clipped 40 min using microaneurysm clamps (Fine Science Tools). After removal of the clamps, reperfusion of the kidneys was visually confirmed. The body temperature of the mice was maintained between 37°C and 38°C. Mice were sacrificed at the indicated days post-IRI.

PAS staining and acute tubular injury score

PAS staining was performed with a PAS staining kit (Solarbio, Beijing, China) to evaluate the AKI. Acute tubular injury was assessed by determining the degree of renal tubular injury at the corticomedullary junction in mouse kidney sections or at the renal cortex in human kidney sections. Tubular injury was defined as tubular dilation, tubular atrophy, tubular cast formation, sloughing of TECs, or loss of the brush border and thickening of the tubular basement membrane. The acute tubular injury score was evaluated using the following scoring system: Score 0: no tubular injury; score 1: <25% of tubules injured; score 2: 25%–50% of tubules injured; score 3: 50%–75% of tubules injured; score 4: >75% of tubules injured. The score of each kidney sample was reported as the mean of 10 random high-power (400×) fields. All of the assessments were made by two investigators blinded to experimental conditions.

Determination of serum creatinine

Serum creatinine was determined by an automatic chemistry analyzer (AU480 Chemistry Analyzer, Beckman Coulter, Atlanta, GA, USA). The levels of serum creatinine were expressed as milligrams per deciliter.

Human kidney biopsy samples

To evaluate the relevance of our findings, we used diagnostic renal biopsy samples from 15 patients with AKI (Table S4). Among these patients, 10 had AKI due to severe edema induced by nephrotic syndrome and 5 patients had AKI due to vomiting or diarrhea. Renal biopsies were performed at the First Affiliated Hospital of Guangzhou medical University. Normal kidney tissues adjacent to tumors from the patients who had renal cell carcinoma and underwent nephrectomy were used as normal control. All of the studies involving human kidney sections were approved by the institutional ethics committee at the First Affiliated Hospital of Guangzhou medical University. All of the study participants were provided written informed consent.

Masson's trichrome staining and tubular interstitial fibrosis index

Paraffin-embedded mouse sections were prepared by routine procedure. Renal sections were subjected to Masson's trichrome staining for evaluating collagen deposition and fibrotic lesions, as described previously.[16] To analyze the level of tubulointerstitial fibrosis, Masson's trichrome-stained sections from each kidney were graded according to the following scale: 0, no evidence of tubulointerstitial fibrosis; 1, <25% involvement; 2, 25%−50% involvement; and 3, >50% involvement. The score of each kidney sample was reported as the mean of 10 random high-power (400×) fields.

Next-generation sequencing of lncRNA

Total RNAs were isolated from isolated tubules of mice with the TRIzol reagent (Thermo Fisher Scientific). Whole transcriptome deep sequencing (RNA-seq) was performed and analyzed by KangChen Bio-tech (Shanghai, China) with the Illumina HiSeq 4000 sequencing system. Briefly, library preparation was performed with the KAPA Stranded RNA-Seq Library Prep Kit (Illumina, San Diego, CA,

USA). The quality control of the RNA-seq library was performed with the Agilent 2100 Bioanalyzer. The processed sequencing reads were mapped to reference genomes (GRCm38/mm10). The FPKM calculation of gene and transcript level was performed using R software (R Foundation for Statistical Computing, Vienna, Austria), and the expression differences of gene and transcript level were calculated respectively to screen out differentially expressed genes between groups. The sequencing data were deposited in the National Center for Biotechnology Information (NCBI) Gene Expression Omnibus database (GSE179506).

mRNA-seq and functional enrichment analysis

To perform the functional enrichment analysis of the differentially expressed mRNAs between the isolated tubules from severe and mild IRI mice, total RNAs were extracted and measured for the quality before the sequencing libraries were constructed with the KAPA stranded RNA-Seq Library Prep Kit (Roche, Basel, Switzerland). The RNA-seq libraries were sequenced with an Illumina X-ten/NovaSeq (Aksomics, Shanghai, China). Sequencing reads were filtered using software FastQC. Clean reads were aligned to the mouse reference genome GRCm38/mm10 (NCBI) using HISAT2 (Hierarchical Indexing for Spliced Alignment of Transcripts), and the gene expression level was calculated using the RSEM software package. To identify differentially expressed mRNAs across samples, the edgeR package was used. We chose mRNAs with a fold change ≥ 2 and $p < 0.05$ in a comparison between the isolated tubules from severe and mild IRI kidney as significant differentially expressed mRNAs. The differentially expressed mRNAs were analyzed with Database for Annotation Visualization and Integrated Discovery (DAVID) for GO enrichment analysis. The enriched biological process (BP) that had $p < 0.05$ was considered significantly enriched. According to the Kyoto Encyclopedia of Genes and Genomes (KEGG) annotation results, the differentially expressed genes were classified by the official classification.

TUNEL assay in kidney sections

Apoptotic cell death was assessed by using TUNEL staining with the DeadEnd Fluorometric Apoptosis Detection System (Promega, Madison, WI, USA) following the manufacturer's instructions. To quantitatively analyze the TUNEL staining-positive TECs in kidney sections, each sample was calculated for the percentage of $TUNEL^+$ TECs in total number of TECs based on 10 random fields under a 40× objective.

Northern blot

Northern blots were performed as previously described.[15] Briefly, total RNA was separated on an agarose-formaldehyde gel. Following separation, the RNAs were transferred from the gel onto a nylon membrane (Solarbio Life Science, Beijing, China), then the membrane was cross-linked and incubated with 5′ digoxin-labeled LNA-modified probes at 52°C overnight. The signaling was visualized with the DIG Northern Starter Kit (Roche) according to the manufacturer's instructions. The probes were synthesized by Exiqon (Vedbæk, Denmark) according to the sequences of the target genes listed in Table S3.

ISH

To determine the expression of *Neat1_2* and *miR-129-5p* in cultured HK2 cells, the FAM-labeled specific probe to *Neat1_2* and the Cy3-labeled specific probe to *miR-129-5p* were designed and synthesized by RiboBio (Guangzhou, China). The signals were detected by the FISH kit (RiboBio) according to the manufacturer's instructions. Briefly, the control or hypoxia-treated cells were fixed in 4% formaldehyde and permeabilized in PBS containing 0.5% Triton X-100. Hybridization was performed in hybridization buffer with specific probes at 37°C overnight in a moist chamber. Cells were then washed with 4× SSC, 2× SSC, and 1× SSC at 42°C. The cells were counterstained with 4,6-diamidino-2-phenylindole (DAPI) (C1006, Beyotime, Shanghai, China). Images were taken by confocal microscopy (Leica TCS SP2 AOBS, Leica Microsystems, Buffalo Grove, IL, USA).

Expression levels of *Neat1_2* in mouse kidneys and human renal biopsy samples were examined with ISH. FISH assay in mouse kidney cryosections was performed to demonstrate whether *Neat1_2* expresses mainly in TECs. Briefly, sections of paraffin-embedded kidney tissue were digested with trypsin (ZSGB-BIO, Beijing, China) and fixed in 4% paraformaldehyde, then hybridized with the 5′ digoxin-labeled LNA-modified *Neat1_2* probe (Exiqon) at 52°C for 16 h. After washing, samples were incubated overnight at 4°C with anti-digoxin monoclonal antibody (ab419, Abcam) followed by incubation of alkaline phosphatase streptavidin (ZB2422, ZSGB-BIO) and then were stained with nitro blue tetrazolium/5-bromo-4-chloro-3-indolyl-phosphate (Beyotime). The proportion of the positive cytoplasmic staining TECs was calculated in sections from each kidney in 10 random fields under a 20× objective.

For FISH assays, after hybridization, the cryosections were incubated overnight with anti-digoxigenin-rhodamine (11207750910, Roche) followed by stained with anti-*Lotus tetragonolobus* lectin (LTL) (FL-1321, Vector Laboratories, Newark, CA, USA). After washing with Tris-buffered saline with 0.1% Tween 20 detergent (TBS-T), slides were incubated with DAPI (C1006, Beyotime). Images were taken by confocal microscopy (Leica).

Western blot analysis

The proteins from cultured cells or tissues were extracted using RIPAlysis buffer (Beyotime) with protease inhibitor (Sigma) and quantified with the bicinchoninic acid BCA protein quantitation kit (Thermo Fisher Scientific). Western blot analyses were conducted as described previously.[16] The primary antibodies used were as follows: anti-FADD (2782S, Cell Signaling Technology, Danvers, MA, USA; AV30294, Sigma), anti-caspase-8 (4790S, Cell Signaling Technology), anti-cleaved caspase-8 (8592S and 9748S, Cell Signaling Technology), anti-caspase-3 (9662S, Cell Signaling Technology), anti-cleaved caspase-3 (9661S, Cell Signaling Technology), anti-caspase-7 (9492S, Cell Signaling Technology), anti-cleaved caspase-7 (8438S, Cell Signaling Technology), anti-Bax (5023S and 14796S,

Cell Signaling Technology), anti-Bcl2 (3498S, Cell Signaling Technology), anti-β-actin (4970S, Cell Signaling Technology), anti-p53 (2524S, Cell Signaling Technology), anti-phospho-p53 (Ser15) (9284S, Cell Signaling Technology), anti-fibronectin (F3648, Sigma), anti-collagen I (72026S, Cell Signaling Technology), anti-αSMA (alpha smooth muscle actin; 19245S, Cell Signaling Technology), anti-Rela (SAB5701125, Sigma), anti-E-cadherin (14472S, Cell Signaling Technology), anti-vimentin (5741S, Cell Signaling Technology), and anti-FSP-1 (13018S, Cell Signaling Technology). Western blot images were quantitatively analyzed using the ImageJ program (NIH, Bethesda, MD, USA).

RNA immunoprecipitation

The MagnaRIP RNA-Binding Protein Immunoprecipitation Kit (Merck Millipore, Burlington, MA, USA) was applied according to the manufacturer's instructions. The whole-cell lysates were incubated with beads coated with antibody against Argonaute-2 (AGO2) (2897S, Cell Signaling Technology) and control immunoglobulin G (IgG) (3900S, Cell Signaling Technology) in a rotator (MiuLab, Hangzhou, China) at 4°C overnight. Next, the co-immunoprecipitated RNA was isolated for the detection of *Neat1_2* and *miR-129-5p* by qPCR.

Biotin-coupled miRNA capture

The 3′ end biotinylated *miR-129-5p* mimics or control RNA (Ribio, Beijing, China) was transfected into 1×10^6 HK2 cells at a final concentration of 50 nM for 48 h before harvest. Then, 0.5 mL lysis buffer (5 mM $MgCl_2$, 100 mM KCl, 20 mM Tris [pH 7.5], 0.3% NP-40 and 50 U of RNase OUT (Invitrogen) was added into the cell lysates and incubated on ice for 10 min. The biotin-coupled RNA complexes were pulled down by incubating the cell lysates with streptavidin-coated magnetic beads (Thermo Fisher Scientific). The abundance of *Neat1_2* in the complex was evaluated by qPCR assays.

DNA pull down and liquid chromatography-tandem mass spectrometry

HK2 cells were grown to 80% confluency and cultured in low-glucose DMEM/Ham's F12 medium (Invitrogen) at 37°C for 24 h in a hypoxia chamber (1% O_2, 5% CO_2, 94% N_2). Then, cells were washed with cold PBS, trypsinized, and collected by centrifugation. The nuclear lysates of the collected cells were extracted with PARIS kit (Thermo Fisher Scientific) according to the manufacturer's instructions. Dynabeads C1 streptavidin magnetic beads (Thermo Fisher Scientific) were washed 3 times with cold B&W buffer (5 mM Tris pH 7.5, 1 M NaCl, 0.5 mM EDTA). Beads (0.5 mL) were incubated with a 100-μg biotinylated promoter sequence of *Neat1* (−1∼−2,000 bp) for 1 h at room temperature. DNA pull down was performed by co-incubation of nuclear extracts with magnetic beads-DNA complexes overnight at 4°C. The negative control assay was performed by incubating magnetic beads with equal amounts of nuclear extracts. Beads were washed 5 times with cold B&W buffer and resuspended with 100 μL elution buffer, followed by reaction with 20 U benzonase nucleases at 37°C for 1 h and separated by SDS-PAGE. Silver staining was performed with the Pierce Silver Stain kit (Thermo Fisher Scientific). A protein band (40–55 kDa) that was specifically enriched in the complexes pulled down by beads-*Neat1* promoter was analyzed by mass spectrometry and protein identification (Bioprofile Biotechnology, Shanghai, China). The gel-containing beads-pull down complexes, at the corresponding size and position, were used as negative control. The mass spectra were submitted to Proteome Discoverer (version 2.4.1.15) for peptide identification and searched against the *Homo sapiens* Uniprot FASTA database. The specific proteins pulled down by beads-*Neat1* promoter were the proteins that were not included in the negative control group (Data S2).

ChIP

ChIP was performed with the Magna ChIP HiSens Chromatin IP Kit (Merck Millipore) according to the manufacturer's instructions as previously described.[16] In brief, control or hypoxia-treated HK2 cells were cross-linked with 1% formaldehyde (Thermo Fisher Scientific) for 30 min at 37°C, quenched with glycine, and then sonicated with an Ultrasonic Cell Disruptor (Diagenode, Liege, Belgium) to generate 300–600 bp DNA fragments. Immunoprecipitation was performed with an antibody against p53 (2524S, Cell Signaling Technology). The binding of the *Neat1_2* promoter to p53 or IgG was quantified by qPCR. The specific primers are listed in Table S3.

Cell apoptosis assays

To perform the apoptosis assay, cells subjected to different treatments were stained with annexin V and propidium iodide (PI) for 30 min with the FITC Annexin V Apoptosis Detection Kit II (BD Biosciences, Franklin Lakes, NJ, USA) according to the manufacturer's instructions. Data were analyzed using FlowJo software.

Gene gain-of-function and loss-of-function analysis *in vivo*

Gain-of-function for Neat1_2

The full length of *Neat1_2* was broken into continuous fragments and cloned into GV411 vector separately. After sequencing ensured accuracy of the vector, AAV9 was produced and titrated by Genechem Biotechnology (Shanghai, China). AAV9 (1×10^{11} copies) harboring either the sequences of *Neat1_2* or the empty vector was injected through the bilateral renal veins of mice to deliver *Neat1_2* in the kidney. Briefly, under general anesthesia, the bilateral kidneys of the mouse were exposed. The renal veins were clamped by microaneurysm clamp, and AAV particles diluted in 100 μL saline were injected into the veins through a 31-G needle. The clamp was removed 15 min after injection followed by suture of the incision.

Loss-of-function for Neat1_2

The siRNA targeting *Neat1_2* was inserted into a GV480 vector, which was co-expressed with mCherry, and AAV9 was packaged, purified, and titrated by Genechem Biotechnology. AAV9 (1×10^{11} copies) harboring either the siRNA or the scramble sequence was injected through the bilateral renal veins of mice to knock down *Neat1_2* in the kidney.

Loss-of-function for miR-129-5p

To inhibit *miR-129-5p in vivo*, C57BL/6 mice transfected with AAV9-si*Neat1_2* were injected with anti-mmu-*miR-129-5p* LNA (Exiqon) through intravenous injection 2 days before renal IRI at a dose of 20 mg/kg. Scrambled sequence LNA was used as the control.

Luciferase reporter assays

To verify whether *Neat1_2* is transcribed by p53, we cloned the full-length or the truncated sequences between −1 and −2,000 bp into pGL3-enhancer vector (Merck Millipore). To verify the binding site of p53 on the promoter region of *Neat1_2*, we cloned the promoter sequence of *Neat1_2* from −1 to −2,000 bp and generated the mutation site in the region between −1,459 and −1,475 bp, and then inserted them separately into the pGL3-enhancer vector (Figure 1N). The sequences of all of the constructs were confirmed by DNA sequencing. HK2 cells were transiently transfected with pRL-TK-renilla-luciferase plasmid and pGL3-enhancer vector carrying WT or mutated promoter constructs. After treatment with hypoxia or normoxia for 24 h, cells were collected and luciferase activity was measured with the Dual-Luciferase Reporter Assay System (Promega) according to the manufacturer's instructions. Firefly luciferase activity was divided by renilla luciferase activity in the same sample to calculate the transfection efficiency, which was then used to normalize the data.

To validate the *miR-129-5p* binding ability to *Neat1_2*, *FADD*, *CASP-3*, and *CASP-8*. The sequences of *Neat1_2*, *FADD-3′UTR*, *CASP-3-3′UTR*, *CASP-8-3′UTR*, and their *miR-129-5p* binding sites mutants were synthesized and cloned to luciferase reporter vector psiCHECK2 (Hanbio Biotechnology, Wuhan, China), called *Neat1_2*-WT, *Neat1_2*-Mut, *FADD*-WT, *FADD*-Mut, *CASP-3*-WT, *CASP-3*-Mut, *CASP-8*-WT, and *CASP-8*-Mut, respectively. To exclude that *miR-129-5p* directly regulated the expression of *Bax* and *CASP-7*. The sequences of the 3′ UTR of *Bax* and *CASP-7* were synthesized and cloned to luciferase reporter vector psiCHECK2, respectively. The experimental protocol follows the manufacturer's instructions of the Promega Dual-Luciferase Reporter Assay System.

Immunofluorescence staining

To demonstrate the efficacy of AAV9 *in vivo*, kidney cryosections from mice injected with AAV9-si*Neat1_2* were fixed in 4% formaldehyde, permeabilized with 0.5% Triton X-100, and stained with anti-LTL (FL-1321, Vector Laboratories). After washing with TBS-T, slides were incubated with DAPI (C1006, Beyotime). Images were taken by confocal microscopy (Leica TCS SP2 AOBS, Leica Microsystems).

Immunohistochemical staining

Immunohistochemistry was performed as previously described.[15] Briefly, after dewaxing and rehydration, antigen retrieval was performed by the microwave method. The sections were then incubated overnight at 4°C with primary antibodies against FADD (ab216506, Abcam, Cambridge, UK), caspase-3 (ab184787, Abcam), cleaved caspase-3 (AB3623, Sigma), fibronectin (F3648, Sigma), collagen I (BA0325, Boster, Wuhan, China), αSMA (ab5694, Abcam), and F4/80 (70076S, Cell Signaling Technology). After thorough washing with PBS buffer, the sections were treated with goat anti-mouse/rabbit horseradish peroxidase (HRP)-conjugated antibodies and visualized by DAB staining (Boster). The staining scores of protein expression were evaluated according to the percentage of the area that stained positive in 10 random fields under a 40× objective. The percentage of positively stained areas in sections from each kidney were scored as follows: 0, no positive stained area; 1, <10%; 2, 10%–25%; 3, 25%–50%; and 4, >50% area staining positive. The staining score in each kidney was the sum of scores of the 10 random fields.

Statistical analysis

Continuous variables were expressed as means ± SD. Data were tested for normality using the Kolmogorov-Smirnov test and variance homogeneity using Levene's test. For comparing normally distributed continuous variables, we used the two-tailed Student's *t* test or one-way ANOVA with a Tukey's post hoc test. For comparing variables that were not normally distributed, we used the Mann-Whitney *U* test. Pearson correlation analyzed the associations between *Neat1_2* expression and acute tubular injury score or percentage of TUNEL staining-positive cells. $p < 0.05$ was considered statistically significant.

DATA AVAILABILITY

RNA-seq data that support the findings of this study have been deposited in GEO (GSE179506).

SUPPLEMENTAL INFORMATION

Supplemental information can be found online at https://doi.org/10.1016/j.ymthe.2022.05.019.

ACKNOWLEDGMENTS

This work was supported by the National Natural Science Foundation of China (grant nos. 82000651 and 82170691, to P.W.); the Outstanding Youths Development Scheme of Nanfang Hospital, Southern Medical University (grant no. 2020J008, to P.W.); the Guangdong Basic and Applied Basic Research Foundation (grant nos. 2019A1515110490 and 2022A1515012209, to P.W.); the China Postdoctoral Science Foundation (grant nos. 2020M672742 and 2020T130280, to P.W.); and the Medical Scientific Research Foundation of Guangdong Province of China (grant no. A2021051, to T.M.).

AUTHOR CONTRIBUTIONS

T.M. participated in study design and manuscript writing. T.M., H. Li, H. Liu, Y.P., and Z.D. conducted the experiments. T.M., Z.D., and N.J. analyzed the data. Z.C. provided guidance with the experiments and edited the manuscript. P.W. designed the study and wrote the paper.

DECLARATION OF INTERESTS

The authors declare no competing interests.

REFERENCES

1. Kalantar-Zadeh, K., Jafar, T.H., Nitsch, D., Neuen, B.L., and Perkovic, V. (2021). Chronic kidney disease. Lancet *398*, 786–802. https://doi.org/10.1016/s0140-6736(21)00519-5.

2. Liu, Y. (2006). Renal fibrosis: new insights into the pathogenesis and therapeutics. Kidney Int. *69*, 213–217. https://doi.org/10.1038/sj.ki.5000054.

3. Chawla, L.S., Eggers, P.W., Star, R.A., and Kimmel, P.L. (2014). Acute kidney injury and chronic kidney disease as interconnected syndromes. N. Engl. J. Med. *371*, 58–66. https://doi.org/10.1056/NEJMra1214243.

4. Ishani, A., Xue, J.L., Himmelfarb, J., Eggers, P.W., Kimmel, P.L., Molitoris, B.A., and Collins, A.J. (2009). Acute kidney injury increases risk of ESRD among elderly. J. Am. Soc. Nephrol. *20*, 223–228. https://doi.org/10.1681/asn.2007080837.

5. Wald, R., Quinn, R.R., Luo, J., Li, P., Scales, D.C., Mamdani, M.M., and Ray, J.G. (2009). Chronic dialysis and death among survivors of acute kidney injury requiring dialysis. Jama *302*, 1179. https://doi.org/10.1001/jama.2009.1322.

6. Cao, W., Cui, S., Yang, L., Wu, C., Liu, J., Yang, F., Liu, Y., Bin, J., and Hou, F.F. (2017). Contrast-enhanced ultrasound for assessing renal perfusion impairment and predicting acute kidney injury to chronic kidney disease progression. Antioxid. Redox Signal *27*, 1397–1411. https://doi.org/10.1089/ars.2017.7006.

7. Liu, B.C., Tang, T.T., Lv, L.L., and Lan, H.Y. (2018). Renal tubule injury: a driving force toward chronic kidney disease. Kidney Int. *93*, 568–579. https://doi.org/10.1016/j.kint.2017.09.033.

8. Nasu, K., Kawakami, T., Shinohara, A., Sakamoto, T., and Nangaku, M. (2020). Munc18-1-interacting protein 3 mitigates renal fibrosis through protection of tubular epithelial cells from apoptosis. Nephrol. Dial. Transpl. *35*, 576–586. https://doi.org/10.1093/ndt/gfz177.

9. Grgic, I., Campanholle, G., Bijol, V., Wang, C., Sabbisetti, V.S., Ichimura, T., Humphreys, B.D., and Bonventre, J.V. (2012). Targeted proximal tubule injury triggers interstitial fibrosis and glomerulosclerosis. Kidney Int. *82*, 172–183. https://doi.org/10.1038/ki.2012.20.

10. Filep, J.G. (2016). Attenuation of lung ischemia-reperfusion injury: silencing the Fas gene. Crit. Care Med. *44*, 1619–1620. https://doi.org/10.1097/ccm.0000000000001687.

11. Date, T., Mochizuki, S., Belanger, A.J., Yamakawa, M., Luo, Z., Vincent, K.A., Cheng, S.H., Gregory, R.J., and Jiang, C. (2003). Differential effects of membrane and soluble Fas ligand on cardiomyocytes: role in ischemia/reperfusion injury. J. Mol. Cell Cardiol. *35*, 811–821. https://doi.org/10.1016/s0022-2828(03)00139-1.

12. Linkermann, A., Chen, G., Dong, G., Kunzendorf, U., Krautwald, S., and Dong, Z. (2014). Regulated cell death in AKI. J. Am. Soc. Nephrol. *25*, 2689–2701. https://doi.org/10.1681/asn.2014030262.

13. Del Rio, M., Imam, A., DeLeon, M., Gomez, G., Mishra, J., Ma, Q., Parikh, S., and Devarajan, P. (2004). The death domain of kidney ankyrin interacts with Fas and promotes Fas-mediated cell death in renal epithelia. J. Am. Soc. Nephrol. *15*, 41–51. https://doi.org/10.1097/01.asn.0000104840.04124.5c.

14. Hamar, P., Song, E., Kökény, G., Chen, A., Ouyang, N., and Lieberman, J. (2004). Small interfering RNA targeting Fas protects mice against renal ischemia-reperfusion injury. Proc. Natl. Acad. Sci. U S A. *101*, 14883–14888. https://doi.org/10.1073/pnas.0406421101.

15. Wang, P., Chen, W., Ma, T., Lin, Z., Liu, C., Liu, Y., and Hou, F.F. (2020). lncRNA lnc-TSI inhibits metastasis of clear cell renal cell carcinoma by suppressing TGF-β-induced epithelial-mesenchymal transition. Mol. Ther. Nucleic Acids *22*, 1–16. https://doi.org/10.1016/j.omtn.2020.08.003.

16. Wang, P., Luo, M.L., Song, E., Zhou, Z., Ma, T., Wang, J., Jia, N., Wang, G., Nie, S., Liu, Y., and Hou, F. (2018). Long noncoding RNA lnc-TSI inhibits renal fibrogenesis by negatively regulating the TGF-β/Smad3 pathway. Sci. Transl Med. *10*, eaat2039. https://doi.org/10.1126/scitranslmed.aat2039.

17. Wang, Y., Jiang, R., Wang, Q., Li, Y., Sun, Z., and Zhao, H. (2021). Silencing LINC01021 inhibits gastric cancer through upregulation of KISS1 expression by blocking CDK2-dependent phosphorylation of CDX2. Mol. Ther. Nucleic Acids *24*, 832–844. https://doi.org/10.1016/j.omtn.2021.01.025.

18. Ge, Y., Wang, J., Wu, D., Zhou, Y., Qiu, S., Chen, J., Zhu, X., Xiang, X., Li, H., and Zhang, D. (2019). lncRNA NR_038323 suppresses renal fibrosis in diabetic nephropathy by targeting the miR-324-3p/DUSP1 Axis. Mol. Ther. Nucleic Acids *17*, 741–753. https://doi.org/10.1016/j.omtn.2019.07.007.

19. Liu, D., Liu, Y., Zheng, X., and Liu, N. (2021). c-MYC-induced long noncoding RNA MEG3 aggravates kidney ischemia-reperfusion injury through activating mitophagy by upregulation of RTKN to trigger the Wnt/β-catenin pathway. Cell Death Dis. *12*, 191. https://doi.org/10.1038/s41419-021-03466-5.

20. Haddad, G., Kölling, M., Wegmann, U.A., Dettling, A., Seeger, H., Schmitt, R., Soerensen-Zender, I., Haller, H., Kistler, A.D., Dueck, A., et al. (2021). Renal AAV2-mediated overexpression of long non-coding RNA H19 attenuates ischemic acute kidney injury through sponging of microRNA-30a-5p. J. Am. Soc. Nephrol. *32*, 323–341. https://doi.org/10.1681/asn.2020060775.

21. Yang, L., Besschetnova, T.Y., Brooks, C.R., Shah, J.V., and Bonventre, J.V. (2010). Epithelial cell cycle arrest in G2/M mediates kidney fibrosis after injury. Nat. Med. *16*, 535–543. https://doi.org/10.1038/nm.2144.

22. Xiao, L., Zhou, D., Tan, R.J., Fu, H., Zhou, L., Hou, F.F., and Liu, Y. (2016). Sustained activation of wnt/β-catenin signaling drives AKI to CKD progression. J. Am. Soc. Nephrol. *27*, 1727–1740. https://doi.org/10.1681/asn.2015040449.

23. Zhou, Q., Guo, H., Yu, C., Huang, X.R., Liang, L., Zhang, P., Yu, J., Zhang, J., Chan, T.F., Ma, R.C.W., and Lan, H.Y. (2021). Identification of Smad3-related transcriptomes in type-2 diabetic nephropathy by whole transcriptome RNA sequencing. J. Cell Mol Med. *25*, 2052–2068. https://doi.org/10.1111/jcmm.16133.

24. Tang, P.M.K., Zhang, Y.Y., Mak, T.S.K., Tang, P.C.T., Huang, X.R., and Lan, H.Y. (2018). Transforming growth factor-β signalling in renal fibrosis: from Smads to non-coding RNAs. J. Physiol. *596*, 3493–3503. https://doi.org/10.1113/jp274492.

25. Zhou, K.R., Liu, S., Sun, W.J., Zheng, L.L., Zhou, H., Yang, J.H., and Qu, L.H. (2017). ChIPBase v2.0: decoding transcriptional regulatory networks of non-coding RNAs and protein-coding genes from ChIP-seq data. Nucleic Acids Res. *45*, D43–D50. https://doi.org/10.1093/nar/gkw965.

26. Fornes, O., Castro-Mondragon, J.A., Khan, A., van der Lee, R., Zhang, X., Richmond, P.A., Modi, B.P., Correard, S., Gheorghe, M., Baranašić, D., et al. (2020). Jaspar 2020: update of the open-access database of transcription factor binding profiles. Nucleic Acids Res. *48*, D87–D92. https://doi.org/10.1093/nar/gkz1001.

27. Komarov, P.G., Komarova, E.A., Kondratov, R.V., Christov-Tselkov, K., Coon, J.S., Chernov, M.V., and Gudkov, A.V. (1999). A chemical inhibitor of p53 that protects mice from the side effects of cancer therapy. Science *285*, 1733–1737. https://doi.org/10.1126/science.285.5434.1733.

28. Peng, F., Gong, W., Li, S., Yin, B., Zhao, C., Liu, W., Chen, X., Luo, C., Huang, Q., Chen, T., et al. (2021). circRNA_010383 acts as a sponge for miR-135a, and its downregulated expression contributes to renal fibrosis in diabetic nephropathy. Diabetes *70*, 603–615. https://doi.org/10.2337/db20-0203.

29. Ke, L., Yang, D.C., Wang, Y., Ding, Y., and Gao, G. (2020). AnnoLnc2: the one-stop portal to systematically annotate novel lncRNAs for human and mouse. Nucleic Acids Res. *48*, W230–W238. https://doi.org/10.1093/nar/gkaa368.

30. Li, J.H., Liu, S., Zhou, H., Qu, L.H., and Yang, J.H. (2014). starBase v2.0: decoding miRNA-ceRNA, miRNA-ncRNA and protein-RNA interaction networks from large-scale CLIP-Seq data. Nucleic Acids Res. *42*, D92–D97. https://doi.org/10.1093/nar/gkt1248.

31. Wu, Y., Li, P., Liu, L., Goodwin, A.J., Halushka, P.V., Hirose, T., Nakagawa, S., Zhou, J., Liu, M., and Fan, H. (2022). lncRNA Neat1 regulates neuronal dysfunction post-sepsis via stabilization of hemoglobin subunit beta. Mol. Ther. https://doi.org/10.1016/j.ymthe.2022.03.011.

32. Ferenbach, D.A., and Bonventre, J.V. (2015). Mechanisms of maladaptive repair after AKI leading to accelerated kidney ageing and CKD. Nat. Rev. Nephrol. *11*, 264–276. https://doi.org/10.1038/nrneph.2015.3.

33. Chawla, L.S., and Kimmel, P.L. (2012). Acute kidney injury and chronic kidney disease: an integrated clinical syndrome. Kidney Int. *82*, 516–524. https://doi.org/10.1038/ki.2012.208.

34. Chawla, L.S., Amdur, R.L., Amodeo, S., Kimmel, P.L., and Palant, C.E. (2011). The severity of acute kidney injury predicts progression to chronic kidney disease. Kidney Int. *79*, 1361–1369. https://doi.org/10.1038/ki.2011.42.

35. Rabb, H., Ramirez, G., Saba, S.R., Reynolds, D., Xu, J., Flavell, R., and Antonia, S. (1996). Renal ischemic-reperfusion injury in L-selectin-deficient mice. Am. J. Physiol. *271*, F408–F413. https://doi.org/10.1152/ajprenal.1996.271.2.F408.

36. Humphreys, B.D., Valerius, M.T., Kobayashi, A., Mugford, J.W., Soeung, S., Duffield, J.S., McMahon, A.P., and Bonventre, J.V. (2008). Intrinsic epithelial cells repair the kidney after injury. Cell Stem Cell *2*, 284–291. https://doi.org/10.1016/j.stem.2008.01.014.

37. Fornari, F., Pollutri, D., Patrizi, C., La Bella, T., Marinelli, S., Casadei Gardini, A., Marisi, G., Baron Toaldo, M., Baglioni, M., Salvatore, V., et al. (2017). In hepatocellular carcinoma miR-221 modulates sorafenib resistance through inhibition of caspase-3-mediated apoptosis. Clin. Cancer Res. *23*, 3953–3965. https://doi.org/10.1158/1078-0432.Ccr-16-1464.

38. Sasaki, Y.T.F., Ideue, T., Sano, M., Mituyama, T., and Hirose, T. (2009). MENε/β noncoding RNAs are essential for structural integrity of nuclear paraspeckles. Proc. Natl. Acad. Sci. U S A. *106*, 2525–2530. https://doi.org/10.1073/pnas.0807899106.

39. Gao, C., Zou, X., Chen, H., Shang, R., and Wang, B. (2020). Long non-coding RNA nuclear paraspeckle assembly transcript 1 (NEAT1)Relieves sepsis-induced kidney injury and lipopolysaccharide (LPS)-Induced inflammation in HK-2 cells. Med. Sci. Monit. *26*, e921906. https://doi.org/10.12659/msm.921906.

40. Wang, W., and Guo, Z.H. (2020). Downregulation of lncRNA NEAT1 ameliorates LPS-induced inflammatory responses by promoting macrophage M2 polarization via miR-125a-5p/TRAF6/TAK1 Axis. Inflammation *43*, 1548–1560. https://doi.org/10.1007/s10753-020-01231-y.

41. Li, C., Liu, Y.F., Huang, C., Chen, Y.X., Xu, C.Y., and Chen, Y. (2020). Long noncoding RNA NEAT1 sponges miR-129 to modulate renal fibrosis by regulation of collagen type I. Am. J. Physiol. Ren. Physiol. *319*, F93–F105. https://doi.org/10.1152/ajprenal.00552.2019.

42. Yang, Y.L., Xue, M., Jia, Y.J., Hu, F., Zheng, Z.J., Wang, L., Si, Z.K., and Xue, Y.M. (2020). Long noncoding RNA NEAT1 is involved in the protective effect of Klotho on renal tubular epithelial cells in diabetic kidney disease through the ERK1/2 signaling pathway. Exp. Mol. Med. *52*, 266–280. https://doi.org/10.1038/s12276-020-0381-5.

43. Huang, S., Xu, Y., Ge, X., Xu, B., Peng, W., Jiang, X., Shen, L., and Xia, L. (2019). Long noncoding RNA NEAT1 accelerates the proliferation and fibrosis in diabetic nephropathy through activating Akt/mTOR signaling pathway. J. Cell Physiol. *234*, 11200–11207. https://doi.org/10.1002/jcp.27770.

44. Liu, L., Zhang, P., Bai, M., He, L., Zhang, L., Liu, T., Yang, Z., Duan, M., Liu, M., Liu, B., et al. (2019). p53 upregulated by HIF-1α promotes hypoxia-induced G2/M arrest and renal fibrosis in vitro and in vivo. J. Mol. Cell Biol. *11*, 371–382. https://doi.org/10.1093/jmcb/mjy042.

45. Zhou, D., Li, Y., Lin, L., Zhou, L., Igarashi, P., and Liu, Y. (2012). Tubule-specific ablation of endogenous β-catenin aggravates acute kidney injury in mice. Kidney Int. *82*, 537–547. https://doi.org/10.1038/ki.2012.173.